TR 225

Technical Report 225

AD708867

THE ISOTHERMAL COMPRESSIBILITY OF FROZEN SOIL AND ICE TO 30 KILOBARS AT -10°C

Edwin Chamberlain
and
Pieter Hoekstra

June 1970

D D C
RECEIVED
JUL 17 1970
C

CONDUCTED FOR
ADVANCED RESEARCH PROJECTS AGENCY
BY

CORPS OF ENGINEERS, U.S. ARMY
COLD REGIONS RESEARCH AND ENGINEERING LABORATORY
HANOVER, NEW HAMPSHIRE

THIS DOCUMENT HAS BEEN APPROVED FOR PUBLIC RELEASE AND SALE; ITS DISTRIBUTION IS UNLIMITED.

43

BEST
AVAILABLE COPY

THE ISOTHERMAL COMPRESSIBILITY OF FROZEN SOIL AND ICE TO 30 KILOBARS AT -10°C

Edwin Chamberlain

and

Pieter Hoekstra

June 1970

CONDUCTED FOR
ADVANCED RESEARCH PROJECTS AGENCY
BY

CORPS OF ENGINEERS, U.S. ARMY
COLD REGIONS RESEARCH AND ENGINEERING LABORATORY
HANOVER, NEW HAMPSHIRE

THIS DOCUMENT HAS BEEN APPROVED FOR PUBLIC RELEASE AND SALE; ITS DISTRIBUTION IS UNLIMITED.

PREFACE

This study was conducted by Mr. Edwin Chamberlain, Research Civil Engineer, Applied Research Branch (Mr. Albert F. Wuori, Chief), Experimental Engineering Division (Mr. Kenneth A. Linell, Chief), and Dr. Pieter Hoekstra, Research Physicist, Earth Sciences Branch (Dr. Duwayne M. Anderson, Chief), Research Division (Dr. Kay F. Sterrett, Chief), U.S. Army Cold Regions Research and Engineering Laboratory.

The research was supported by the Advanced Research Projects Agency of the Department of Defense under ARPA Order 968.

The authors express their gratitude to Mr. Roscoe Perham for his assistance and cooperation in the research program. They specially thank Dr. Douglas Stephens of the Lawrence Radiation Laboratory for his advice and assistance. Specialist 5 Robert Keune prepared the samples and processed the data. His help in completing this work on time was very valuable.

The report was technically reviewed by Mr. L. David Minsk and Mr. Richard McGaw.

The contents of this report are not to be used for advertising, publication, or promotional purposes. Citation of trade names does not constitute an official endorsement or approval of the use of such commercial products.

CONTENTS

ILLUSTRATIONS

ILLUSTRATIONS (Cont'd)

TABLES

SYMBOLS

a, b	Compressibility coefficients
B_a, B_b, B_c, etc.	Volume compre.sibilties of each mineral component
B_r	Reuss average
B_v	Voigt average
D	Depth to upper seal for any test specimen
D_g	Depth to upper seal for gold
D_0	Die bore diameter at atmospheric pressure
D_s	Depth to upper seal for soil or ice specimens
D_t	Die bore diameter at any pressure
E	Young's modulus
F	Piston load
ℓ	Specimen length
n	Porosity
P	True pressure
P_a	Apparent pressure
S	Residual piston displacement for any test specimen
S_c	Set correction
S_g	Residual piston displacement for gold
S_i	Degree of saturation with ice
S_s	Residual piston displacement for soil or ice specimens
v_i^0	Specific volume of ice at atmospheric pressure
v_i^P	Specific volume of ice at any pressure
V/V_0	Relative volume
V_a, V_b, V_c, etc.	Volume percentages of each mineral component
V_a^0	Volume of air voids at atmospheric pressure
V_g^0	Volume of gold at atmospheric pressure
V_i^0	Volume of ice at atmospheric pressure
V_m^0	Volume of mineral solids at atmospheric pressure
V_s^0	Volume of test specimen at atmospheric pressure

SYMBOLS (Cont'd)

V_s^p	Volume of test specimen at any pressure
V_v^0	Volume of voids at atmospheric pressure
α	Ratio of minor to major radius of a rock cavity
ρ_d	Dry density
ρ [illegible]	Total or wet density
Δ_{g+m}	Apparent axial deformation of gold specimen
Δ'_{g+m}	Adjusted axial deformation of gold specimen
Δ_{s+m}	Apparent axial deformation of soil or ice specimen
$\Delta V/V_0$	Change in relative volume
ΔV_0	Change in volume of air
ΔV_g	True change in volume of gold specimen
ΔV_{g+m}	Apparent change in volume of gold specimen
ΔV_i	Change in volume of ice component
ΔV_m	Change in volume of mineral component
ΔV_s	True change in volume of test specimen
ΔV_{s+m}	Apparent change in volume of test specimen

THE ISOTHERMAL COMPRESSIBILITY OF FROZEN SOIL AND ICE TO 30 KILOBARS AT -10C

by

Edwin Chamberlain and Pieter Hoekstra

INTRODUCTION

The objective of this program was to investigate the compressibility of frozen soils and ice in the pressure region of 0 to 30 kbars at -10C. The data were obtained for use in model calculations for mound and cavity growth and shock wave transmission during a nuclear or high-explosive cratering event in frozen ground. The wide variation of the properties of *in situ* frozen soils with location precludes the direct use of the reported test results for a particular site. Therefore, emphasis has been placed on isolating the physical properties of frozen soils that determine the compressibility so that the compressibility of *in situ* frozen soils can be predicted from convenient measurable parameters.

Frozen soils consist of a matrix of mineral grains with pore spaces that may be filled with ice (water) and air. The problem of prediction of compressibilities falls into two categories: those for saturated frozen ground and those for partially saturated frozen ground. For saturated frozen ground the compressibility can be predicted from the constituent components, ice and mineral. The required parameters are the volumetric proportions and the compressibilities of the mineral components and the ice. For partially saturated frozen ground, in addition to these parameters, the closure of the pore spaces due to the crushing of the grains must be evaluated. This problem remains partially unsolved. As will be demonstrated, this appears to be significant only for soil with a low degree of saturation.

Bridgman (1911, 1912, 1914, and 1937) was the first to investigate the compressibility of water and its many ice phases to high pressures. His work is the basis for this discussion. Other investigators (Whalley *et al.*, 1966; Brown and Whalley, 1966; Wilson, *et al.*, 1965) have studied the phase diagram of water in the pressure-temperature plane but have not made volume change observations.

Numerous investigators (Adams and Williamson, 1923; Bassett *et al.*, 1968; Bridgman, 1964; Brown *et al.*, 1967; Stephens, 1964; Stephens and Lilley, 1966; Walsh, 1965, a,b) have studied the compressibility of minerals, soils, and rocks to high pressures.

A piston-die device with which a uniaxial load is imposed on a lead-encapsulated specimen was used for these tests. The die restrains the encapsulated specimen from lateral expansion. Load and deformation measurements are continuously recorded. The compressibility of gold is used as a standard to provide a continuous calibration of the loading apparatus.

The techniques and operational procedures were developed with the aid of personnel of the Lawrence Radiation Laboratory, Livermore, California.

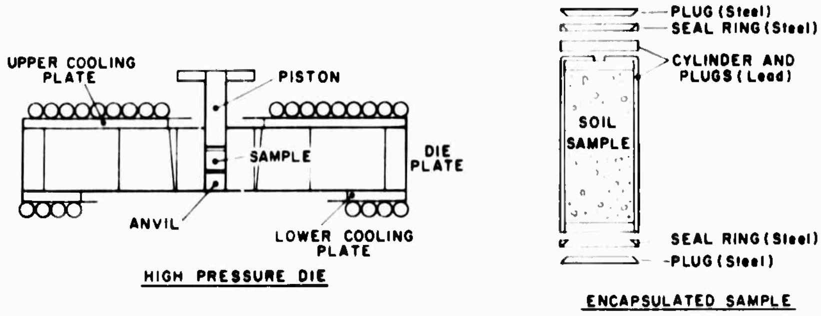

Figure 1. Encapsulated sample and high pressure die.

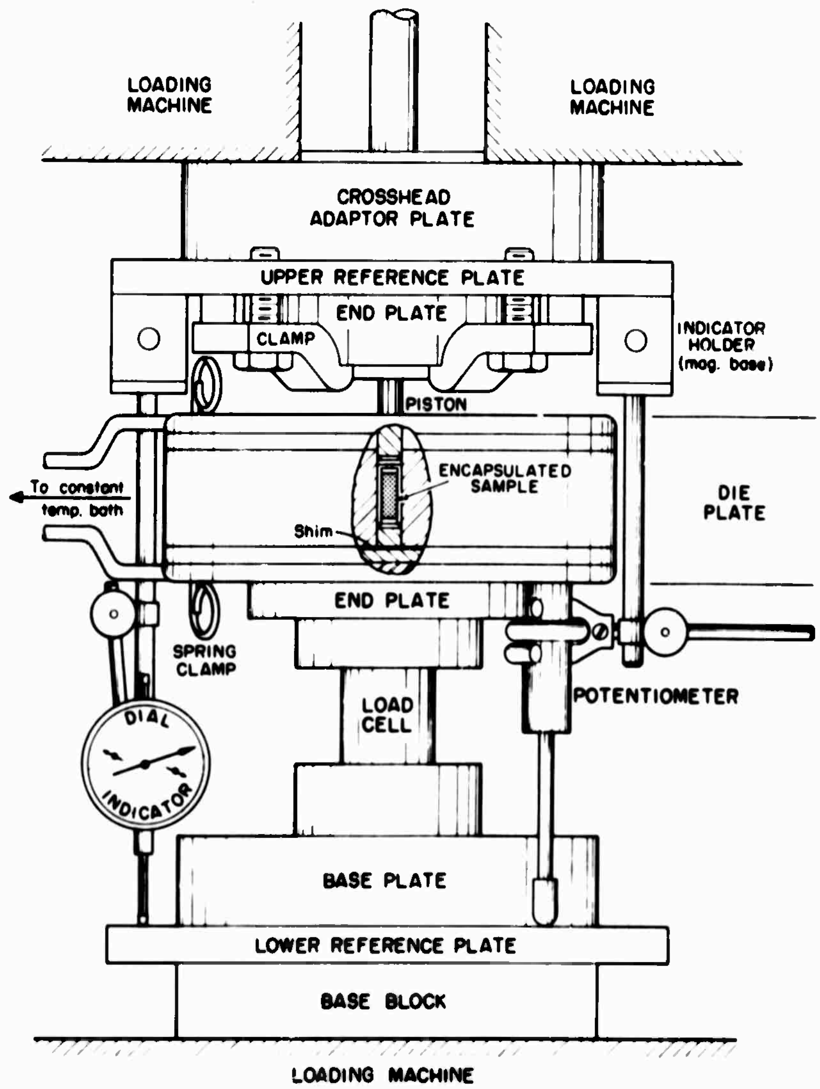

Figure 2. Test apparatus in loading machine.

APPARATUS

The experimental procedure and isothermal compression apparatus are similar to those described by Stephens (1964). The test samples were nominally 1.168 mm in diameter and 2.540 mm long. Each was encapsulated in lead and compressed between two 1.27-cm-diam carbide pistons while confined in the bore of a die plate (see Fig 1 and 2). Hardened steel rings and plugs prevented extrusion of the lead.

The piston was loaded by a Tinius-Olsen Universal, screw-type testing machine (see Fig. 3) at a rate slow enough to obviate any compressive heating effects ($\approx$ 40 min/cycle). The tests were conducted in a coldroom maintained at approximately -10C. To obtain a more precise temperature control, a coolant was circulated through coils attached to the die plate. The coolant was maintained at a temperature of -10 ± 0.5C by a constant temperature bath. The die temperature was sensed by a glass bead thermistor and recorded at intervals. The piston displacement was measured by a linear film potentiometer and the load by a load cell. The load and displacement were recorded on an X-Y plotter. Typical records are shown in Figures 4 and 5.

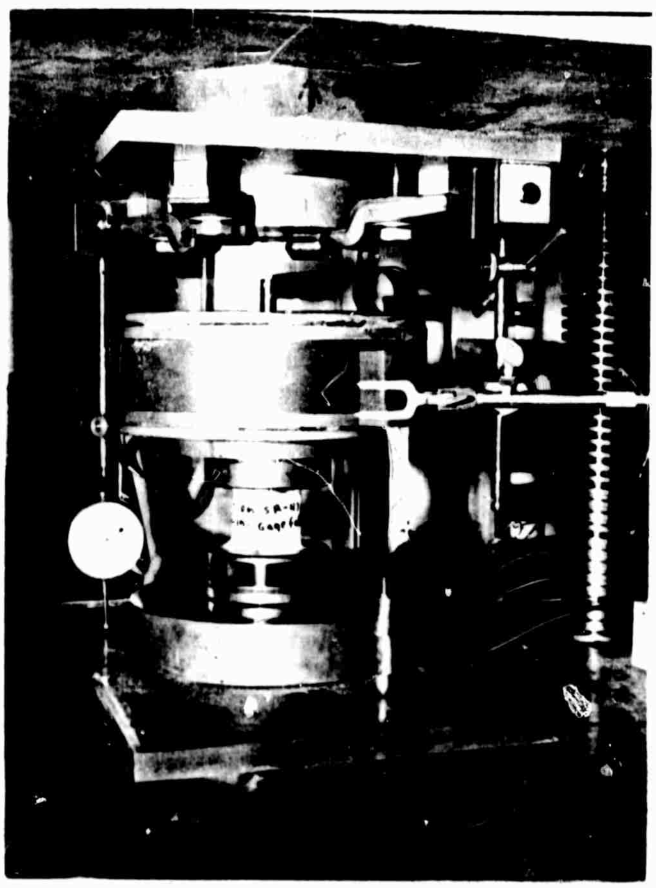

Figure 3. Isothermal compressibility test apparatus.

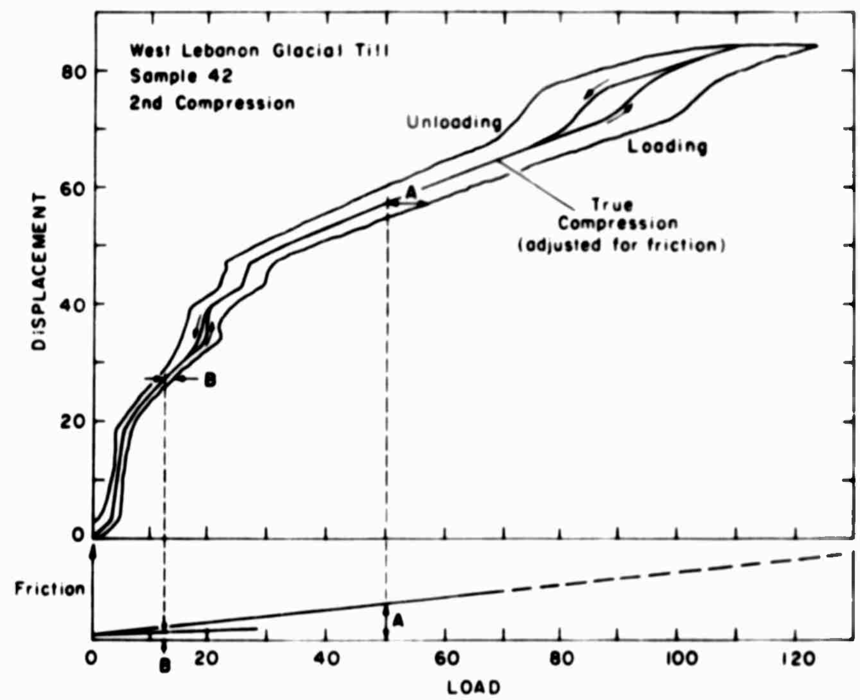

Figure 4. Example of X-Y plots for saturated frozen soil (2nd compression curve).

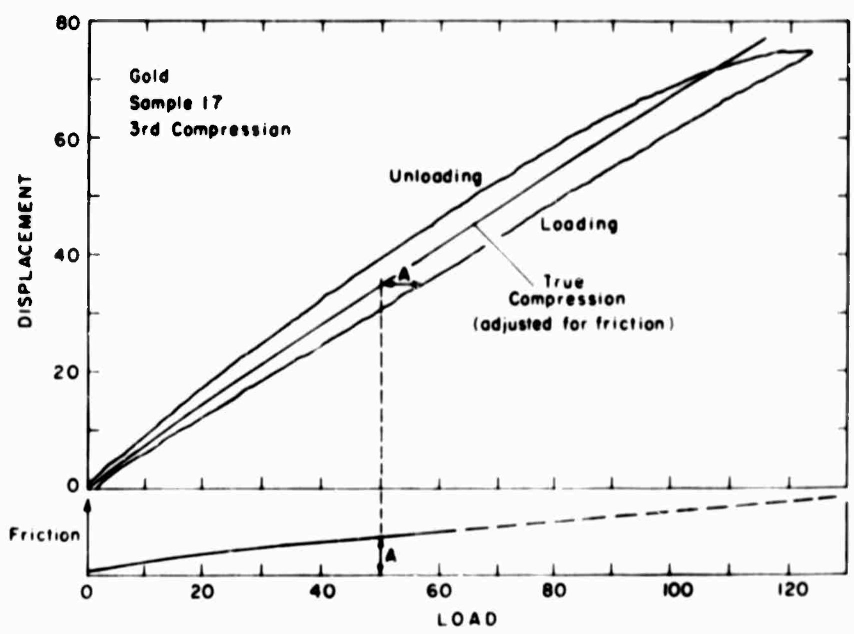

Figure 5. Example of X-Y plots for gold (3rd compression curve).

SAMPLE DESCRIPTION

The relevant index properties and gradations of the materials tested are shown in Table I and Figure 6. The test specimens included two soils: West Lebanon glacial till (WLGT) and Ottawa banding sand (OWS). They were prepared at various degrees of saturation (see Table II). In addition, tests were conducted on clear polycrystalline ice.

Ottawa banding sand

This material was well rounded, well sorted quartz sand with a median diameter of 100 μ and 100% of the material falling between 74 and 149 μ. The material was selected for its high porosity and granular nature, to allow sands and gravels to be modeled. The nature of the test program restricted the maximum particle size to 149 μ. The monomineralic structure of the sand permitted more meaningful comparison with previous results for pure quartz.

West Lebanon glacial till

This material was an extremely well graded till with particles having a maximum diameter of 149 μ and a mean diameter of 36 μ. This gradation contained a high percentage of fine-grained materials in contrast to the gradation of Ottawa banding sand. This material was cut from a boundary till and in its test form was classified silt (ML) according to the Soil Classification System.

Ice

This material was a clear polycrystalline columnar ice having a maximum grain diameter of 0.5 cm, with the c-axis in the direction of compression.

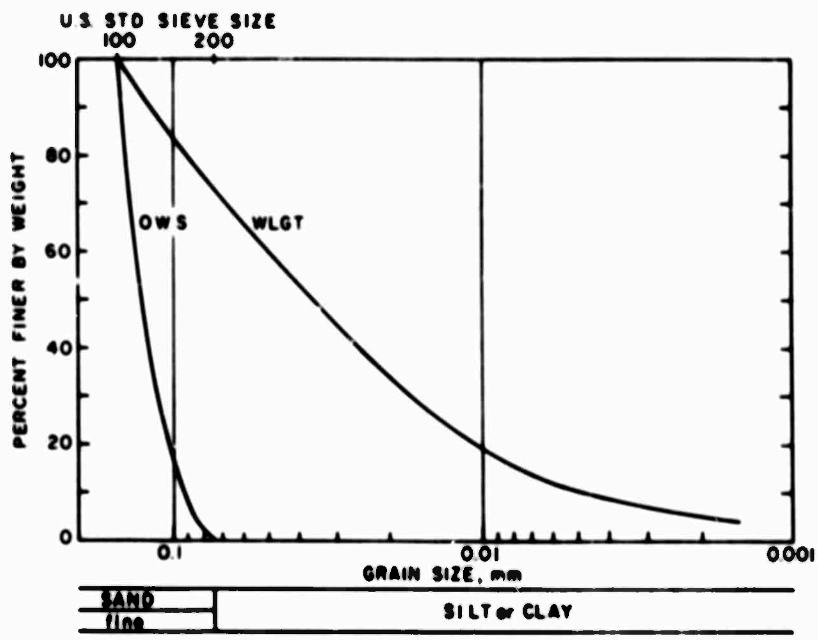

Figure 6. Gradations of the soils tested.

Table I. Material index properties.

Unified Soil Classification	Apparent sp. gr. of solids	Liquid* limit	Plastic* limit	Plasticity* index	Max. dry density (g/cm³)	Optimum water content (%)
			Ottawa banding sand (OWS)			
Sand (SP)	2.68			non-plastic	1.91	
			West Lebanon glacial till (WLGT)			
Silt (ML)	2.86	16.2	18.4	non-plastic	1.91	12.2
			Polycrystalline ice			
	0.917					

* Atterberg limits.

Table II. Summary of sample index properties.

Sample	Porosity	Dry density (g/cm³)	Wet density (g/cm³)	Sat. with ice (%)
		Polycrystalline ice		
11			0.917	
43			.917	
44			.917	
		West Lebanon glacial till		
16	0.367	1.842	2.040	58.3
40	.364	1.852	2.030	57.3
32	.364	1.847	2.172	100.0
42	.358	1.838	2.172	100.0
		Ottawa banding sand		
1	0.378	1.639	2.002	100.0
18	.454	1.438	1.850	100.0
24	.373	1.650	1.985	100.0
27	.373	1.651	1.990	100.0
34	.373	1.651	1.903	75.6
17	.427	1.507	1.940	55.7
28	.373	1.651	1.820	50.9
29	.373	1.651	1.732	25.2
33	.372	1.651	1.732	25.1
35	.372	1.651	1.651	0
31	.372	1.651	1.651	0

SPECIMEN PREPARATION

All soil specimens were prepared in 1.168-cm-ID lead capsules approximately 3.2 cm long, with a wall thickness of 0.051 cm. The specimen length was approximately 2.4 cm. This provided approximately 0.8 cm excess lead for sealing the capsule.

The West Lebanon glacial till specimens were compacted wet by tamping with a 1.15-cm-diam rod. The Ottawa banding sand specimens were compacted dry by vibration. The water content of each specimen was adjusted to the desired value after compaction. Saturated soil specimens were wetted under vacuum. All soil specimens were frozen rapidly in a -10C coldroom and allowed to temper for at least 24 hours.

The ice specimens were frozen from de-aired distilled water in a 7.5-cm-diam plastic tube, machined to size, and placed in the lead capsules. The ice specimens were also tempered for 24 hours at -10C.

TESTING PROCEDURE AND DATA EVALUATION

The primary data were generated by loading and unloading the test samples to and from a pressure of approximately 30 kbars. The load and the corresponding displacement signals were recorded continuously (Fig. 4, 5); the recordings resulted in a loop. This hysteresis was primarily the result of the internal friction in the test specimen, the friction between the lead and the wall of the die bore, and the irreversible closure of soil voids. The techniques used to correct for friction required a closed loop. Thus, each specimen was subjected to several compression cycles until a closed loop was obtained.

The friction was assumed to be equal upon loading and unloading; the average of the two traces represented the compressibility of the material. The friction increased with load. The friction-load relationship was assumed to be unique for each material and not influenced by heat of compression or by structural changes from one cycle to the next. For the partially saturated soil samples, the compressibility was obtained from the first compression curve inasmuch as the subsequent compressions resulted in the irreversible closure of the soil voids. The friction correction for the first compression cycle was obtained from the closed-loop compression curve. For the fully saturated specimens and polycrystalline ice, the friction-corrected closed-loop compression curve was used to compute the sample compressibility. It was assumed that there was no material loss during the loading and unloading cycles. In many cases, the lead capsule containing the soil specimen ruptured, resulting in a moisture loss. These tests were disregarded.

After friction corrections were applied, the loading-unloading curves for the fully saturated specimens and for the ice still exhibited some hysteresis (see Fig.4). This hysteresis is probably related to the rate effects associated with the phase transition.

To correct for mechanical effects external to the sample a differential technique was used: the compressibility of the test specimen was compared with that of gold (Bridgman, 1940; Stephens and Lilley, 1967). Every second sample tested was gold.

To adjust the displacements of the gold samples and the displacements of the test sample to a common datum further correction was applied. Each test sample was preloaded to 50 lb. This load was selected because it was large enough to cause seating of the seals but not so large as to cause significant deformation of the test sample. The load was released, the piston was removed and the depth to the upper seal *D* (See Fig. 7) was measured with a depth micrometer. The piston

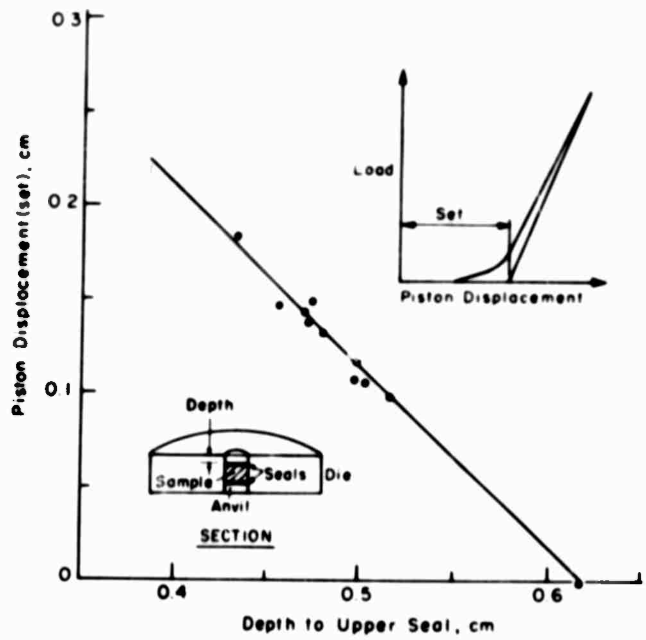

Figure 7. Set correction for gold.

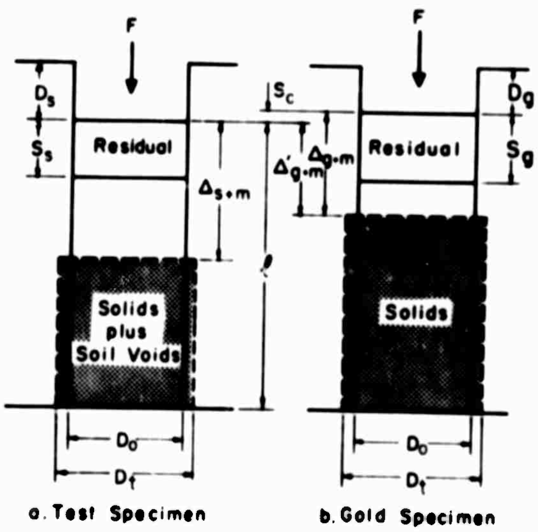

Figure 8. Specimen configuration before and after loading.

was replaced and the test continued. Dial gauge readings were observed at a 50-lb load before and after loading. For the gold samples, the difference between these readings represented the residual displacement required to fill all voids between the seals with lead (the lead would flow under pressure). This piston displacement is called the set S. It is plotted versus D for gold in Figure 7, resulting in the linear expression:

$$S = 0.596 - 0.965D \,. \tag{1}$$

The normalizing of the gold runs to the soil or ice runs is accomplished in the following manner. The set S corresponding to the D for the test sample is found from eq 1. The set correction S_c required to adjust the apparent axial deformation of the gold Λ_{g+m} to the same datum as the test specimen is equal to the difference between the calculated set for the test sample and the measured set for the gold (see Fig 8). The adjusted axial deformation of the gold Λ'_{g+m} at any load F is thus:

$$\Lambda'_{g+m} = \Lambda_{g+m} - S_c \tag{2}$$

The use of this relationship requires that the same total volume of material be contained between the seals for all runs.

Another correction was made to account for the expansion of the die bore under pressure. Stephens and Lilley (1967) gave a table relating the true pressure P to the apparent pressure P_a. Fitting a straight line to their data resulted in the following relationship:

$$P = 0.988\, P_a. \tag{3}$$

The true change in the volume of the test specimen ΔV_s is related to the apparent change in the volume of the test specimen ΔV_{s+m}, the apparent change in the volume of the gold specimen ΔV_{g+m}, and the true change in the volume of the gold specimen ΔV_g in the following expression:

$$\Delta V_s = \Delta V_{s+m} - \Delta V_{g+m} + \Delta V_g. \tag{4}$$

The apparent change in the volume of the gold is equal to the average value for the gold runs before and after loading.

Figure 8 illustrates the specimen configurations before and after loading. The assumed deformation under load is cylindrical. The actual deformed shape is probably more barrel-like, but the difficulties in the evaluation of such a shape lead us to the cylindrical approximation. The apparent change in the volume of the test specimen ΔV_{s+m} is found as follows:

$$\Delta V_{s+m} = \frac{l\,\pi D_0^2}{4} - (l - \Lambda_{s+m})\frac{\pi D_t^2}{4}$$

$$= \frac{\pi}{4}(lD_0^2 - lD_t^2 + \Lambda_{s+m}\, D_t^2). \tag{5}$$

From eq 3 the die bore diameter at any pressure D_t can be related to the die bore diameter at atmospheric pressure D_0 by the following expression:

$$D_t^2 = \frac{D_0^2}{0.988}. \tag{6}$$

Substituting eq 6 in eq 5 gives:

$$\Delta V_{s+m} = \frac{\pi D_0^2}{4}\left(l - \frac{l}{0.988} + \frac{\Lambda_{s+m}}{0.988}\right). \tag{7}$$

Similarly:

$$\Delta V_{g+m} = \frac{\pi D_0^2}{4}\left(l - \frac{l}{0.988} + \frac{\Delta'_{g+m}}{0.988}\right). \tag{8}$$

From Bridgman's (1940) work, we find that ΔV_g at -10C can be expressed in terms of the true pressure P and the initial volume V_g^0 as follows:

$$\Delta V_s = V_g^0\left(5.650 \times 10^{-4} P - 7.235 \times 10^{-7} P^2\right). \tag{9}$$

By substituting 1.27 cm for D_0 eq 4, 7, 8 and 9 reduce to the following expression for the true change in volume of the test specimen ΔV_s:

$$\Delta V_s = 1.282\left(\Lambda_{s+m} - \Lambda'_{g+m}\right) + V_g^0\left(5.650 \times 10^{-4} P - 7.235 \times 10^{-7} P^2\right). \tag{10}$$

The results of the tests reported given in the relative volume V_s^P/V_s^0 versus true pressure P plane. The relative volume is found as follows:

$$V_s^P/V_s^0 = 1 - \Delta V_s/V_s^0. \tag{11}$$

where V_s^0 is the volume of the test specimen at atmospheric pressure and -10C.

THE COMPRESSIBILITY OF ICE AT -10C

Essential to the study of the compressibility of ice is a discussion of the phase diagram of water. Bridgman (1911, 1912, 1914, 1937) published several articles which are still the main source on the phase diagram of water and ice. Although the transition pressures in the phase diagram of water have been studied by others since 1937, these studies have been concerned with properties of water other than compressibility and specific density, the properties of main interest here.

Figure 9 illustrates the phase diagram of water as it is known today. This figure shows that the following transition will occur during the isothermal compressibility of ice at -10C. At a pressure of 1.11 kbars ice I will melt to the liquid phase (water). If the pressure is raised further, the liquid phase will freeze to ice V at a pressure of 4.42 kbars. Upon continued pressure increase, ice V will undergo a polymorphic transition to ice VI at a pressure of 6.25 kbars. Finally ice VI will transform into ice VIII at a pressure of 20.8 kbars. The densities and the specific volumes of the various water phases at different temperatures and pressures may be extracted from Bridgman's data (1911, Tables XXV and XXX; and 1937, Table I).

The specific volume of ice I at 0C and atmospheric pressure is given in Table III as 1.0900 cm³/g. It is assumed that the coefficient of thermal expansion of ice I is small; therefore, the specific volume of ice I at -10C is also 1.0900 cm³/g. From the same table the specific volume of ice I and water at the transition point of 1.11 kbars and -10C can be interpolated as 1.0664 and 0.9544 cm³/g respectively. Other points on the specific volume-pressure curve are determined below.

Table IV gives the specific volume of water and ice V at the transition points for various temperatures. The water-ice V transition at -10C occurs at 4.42 kbars. At a temperature of -10C

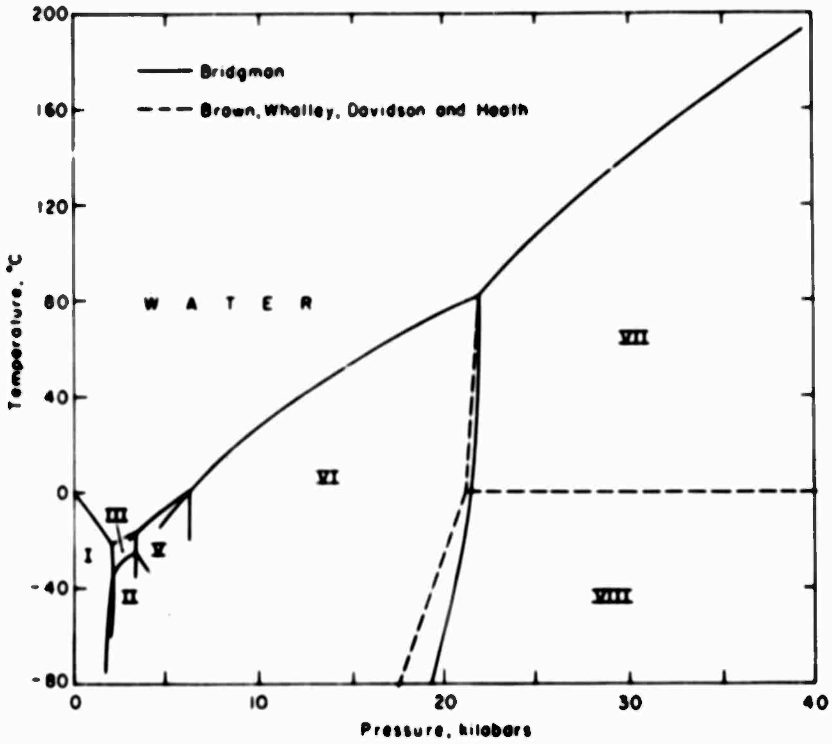

Figure 9. Phase diagram of water in the temperature-pressure plane.

Table III. Specific volume of water and ice I on the equilibrium curve*

Pressure (kg/cm²)	Pressure (kbars)†	Temp. (°C)	Specific vol. of water (cm³/g)	Specific vol. change (cm³/g)	Specific vol. of ice (cm³/g)
0	0.0	0	1.0000	0.0900	1.0900
500	0.49	- 4.1	0.9777	.0998	1.0775
1000	0.98	- 8.7	0.9588	.1096	1.0684
1500	1.47	- 14.0	0.9414	.1201	1.0615
2000	1.96	- 20.3	0.9253	.1318	1.0571

* Bridgman, 1911, taken from Table XXX

† 1 kg cm² = 0.98 × 10⁻³ kbars

Table IV. Specific volume of water and ice V on the equilibrium curve*

Pressure (kg/cm²)	Pressure (kbars) †	Temp. (°C)	Specific vol. of water (cm³/g)	Specific vol. change (cm³/g)	Specific vol. of ice (cm³/g)
3500	3.43	-17.0	0.8870	0.0785	0.8085
4000	3.92	-13.6	.8781	.0733	.8048
4500	4.41	-10.1	.8694	.0681	.8013
5000	4.90	- 7.0	.8610	.0634	.7976
5500	5.39	- 4.2	.8543	.0590	.7953
6000	5.88	- 1.6	.8478	.0549	.7929
6500	6.37	+ 0.6	.8418	.0516	.7902

* Bridgman, 1911, taken from Table XXX

† 1 kg cm² = 0.98 × 10⁻³ kbars

Table V. Specific volume change on the ice V - ice VI equilibrium curve*

Pressure (kg/cm^2)	Pressure (kbars)	Temp. (°C)	Specific vol. change (cm^3/g)
6365	6.24	-20.0	0.03809
6370	6.25	-15.0	.03828
6374	6 25	-10.0	.03847
6377	6.25	- 5.0	.03866
6381	6.25	0.0	.03886

* Bridgman, 1911; taken from Table XXV

† 1 kg/cm^2 = 0.98 × 10^{-3} kbars

Table VI. Specific volume change on the ice VI - ice VII equilibrium curve*

Pressure (kg/cm^2)	Pressure (kbars)†	Temp. (°C)	Specific vol. change (cm^3/g)
22,000	21.6	- 0.0	0.0567
22,250	21.8	20.0	.0570
22,350	21.9	40.0	.0573

* Bridgman, 1937; taken from Table I

† 1 kg/cm^2 = 0.98 × 10^{-3} kbars

and a pressure of 4.42 kbars the specific volume of water is interpolated as 0.8688 cm^3/g. At the same temperature and pressure the specific volume of ice V is interpolated as 0.8012 cm^3/g.

From here on it becomes more difficult to find reliable data. Although Bridgman was most successful in obtaining the volume changes occurring at the phase changes, he had great difficulty measuring the compressibilities of the various phases of water. He did, however, develop specific volume data for ice and water along their equilibrium curves.

From the equilibrium data for the ice V - water transition (Table IV) it is possible to approximate the specific volume of ice V at -10C. At a pressure of 6.25 kbars and a temperature of +0.2C the specific volume of ice V is interpolated as 0.7907 cm^3/g. It is assumed that changes in pressure have a much greater effect than changes in temperature on the specific volume of ice V. The volume change associated with the temperature difference of 10.2C is neglected and the specific volume of ice V at 6.25 kbars and -10C is assumed to be 0.7907 cm^3/g. For the phase transition of ice V to ice VI at -10C, Table V gives the change in volume as 0.03847 cm^3/g. The specific volume of ice VI at -10C and 6.25 kbars is thus 0.7907-0.0385 = 0.7522 cm^3/g.

The volume of ice VIII at -10C and 20.8 kbars is the next calculation to be made. Bridgman did not recognize this phase of ice but thought it to be ice VII. Ice VIII was first observed by Brown and Whalley (1966) and Whalley *et al* (1966), using dielectric techniques. They did not provide data for ice VIII. However, they did suggest that the volume change associated with the ice VII to ice VIII transition is very small (0 ± = 2.78 × 10^{-4} cm^3/g at the ice VI-VII-VIII triple point).

With this in mind, we can approximate the volume of ice VIII. From Bridgman's work, we find that ice VII has a specific volume of approximately 0.60 cm^3/g at room temperature and

Table VII. Compressibility of ice*

Phase	Pressure (kbars)	Specific vol. (cm^3/g)	Relative vol.
	Temperature -10C		
Ice I	0.0	1.0900	1.000
Ice I	1.11	1.0664	0.978
Water	1.11	0.9544	0.876
Water	4.42	0.8688	0.796
Ice V	4.42	0.8012	0.736
Ice V	6.25	0.7907	0.726
Ice VI	6.25	0.7522	0.690
Ice VI	20.8	0.702	0.644
Ice VIII	20.8	0.645	0.592
Ice VIII	49.1	0.60	0.55
	Temperature +5C		
Water	0.0	0.9999	1.0000
Water	6.87	.8370	0.8370
Ice VI	6.87	.7488	0.7488
Ice VI	21.7	.702	0.702
Ice VIII	21.7	.645	0.645
Ice VIII	49.1	.60	0.60

* Calculated from experimental data reported by Bridgman (1911, 1937).

49.1 kbars. We assume that the temperature effect on the specific volume of ice VII is small in comparison with pressure effects. Furthermore, we assume that the volume change associated with the phase transition of ice VII to ice VIII is negligible and that ice VIII exhibits the same compressibility as ice VII. Thus, the specific volume of ice VIII at 49.1 kbars and -10C is 0.60 cm^3/g. The volume change associated with a pressure increase from 19.6 to 44.1 kbars for ice VII is given by Bridgman (1937) as a mean value of 0.039 cm^3/g. We assume that this value is representative in the pressure range of 20.8 to 49.1 kbars at -10C. The resulting volume change for ice VIII at -10C from 49.1 to 20.8 kbars is 0.045 cm^3/g. The specific volume for ice VIII at -10C and 20.8 kbars is, thus, calculated to be 0.60 + 0.045 = 0.645 cm^3/g.

The volume change of ice VII to ice VI at the transition temperature of -10C and 21.4 kbars is extrapolated from Table VI to be 0.057 cm^3/g. We assume that this value holds for the volume change of ice VIII to ice VI at -10C and 20.8 kbars. The resulting specific volume for ice VI at -10C and 20.8 kbars is 0.645 + 0.057 = 0.702 cm^3/g. This completes the calculations for the compressibility of ice at -10C from 0 to 49.1 kbars. The results are tabulated in Table VII and illustrated in Figure 10. The compressibility of each phase is assumed to be linear.

Similar calculations can be performed at other temperatures. In Figure 10, the compressibility of water at +5C is plotted along with the compressibility of ice at -10C. Ice is more compressible than water; therefore, saturated frozen ground would be expected to be more compressible than saturated unfrozen ground.

Figures 11 through 13 and Tables AI-AIII, Appendix A, give test results for the isothermal compressibility of ice. The compressibility as predicted from Bridgman's data is plotted for comparison. The variation of the test results from Bridgman's results can be attributed primarily to rate effects. Bridgman (1911) reported that the change in the volume of the phase changes was

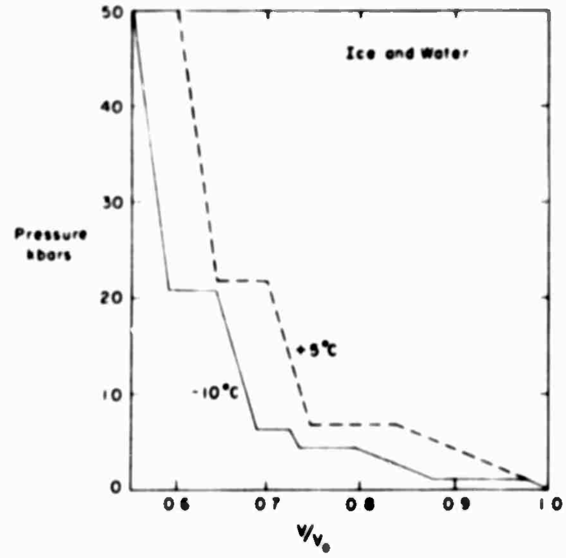

Figure 10. Predicted isothermal compressibility of ice at -10C and water at +5C.

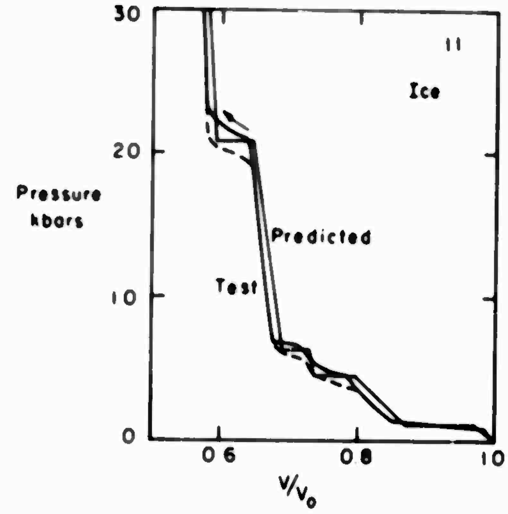

Figure 11. Isothermal compressibility of ice, specimen 11.

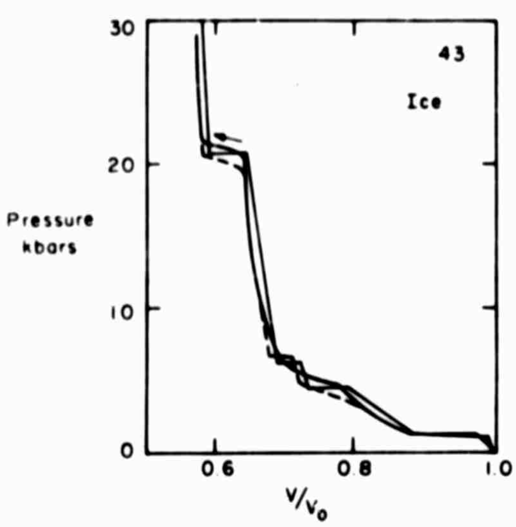

Figure 12. Isothermal compressibility of ice, specimen 43.

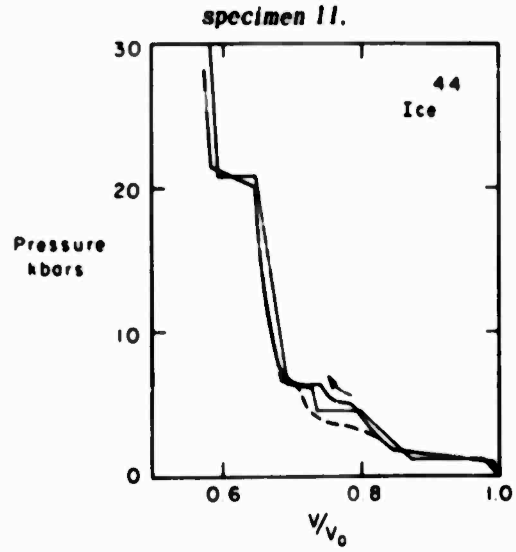

Figure 13. Isothermal compressibility of ice, specimen 44.

time dependent; e.g., the time for completion of the liquid-solid reaction was about two hours on the ice I-liquid boundary. The solid-solid reactions were nearly explosive near the triple point but were slow at other points. The time allotted for the tests reported here ($\approx$ 40 min/cycle) was probably inadequate to allow complete phase transformations at the transition pressures.

The slightly greater compressibility of the results reported might be explained by the presence of microscopic air bubbles. An included air volume of approximately 1% would account for the differences.

Bridgman (1911) found that ice V nucleated only in the presence of glass splinters. Two of the three ice specimens tested showed the liquid-ice V transition. However, for specimen 43 (Fig 12) ice V did not nucleate and the liquid phase froze to ice VI upon loading beyond the liquid-ice V transition. In all tests ice V was observed on the unloading cycle; this is consistent with Bridgman's results.

THE COMPRESSIBILITY OF FROZEN SAND AND SILT AT -10C

The results of the isothermal compressibility tests on frozen sand and silt are given in Appendix A and in Figures 14-28.

It was suggested in the introduction that only a few material properties were needed to estimate the compressibility of frozen ground. This problem has been discussed by Brace (1965) and Stephens (1964) for rocks. The general approach has been to average the compressibilities of the minerals making up the rock. Two kinds of averages have been employed: the Reuss average

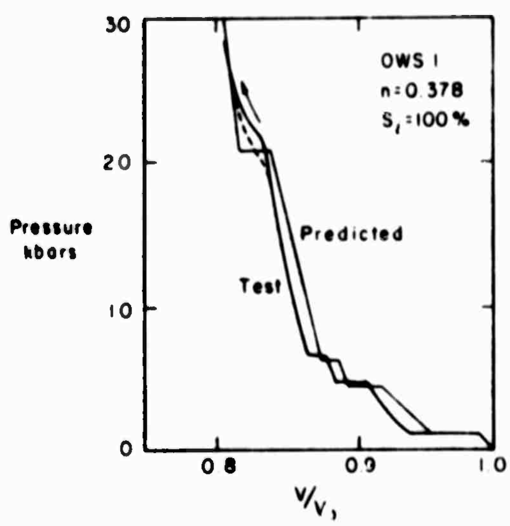

Figure 14. Isothermal compressibility of fully saturated Ottawa banding sand, specimen 1.

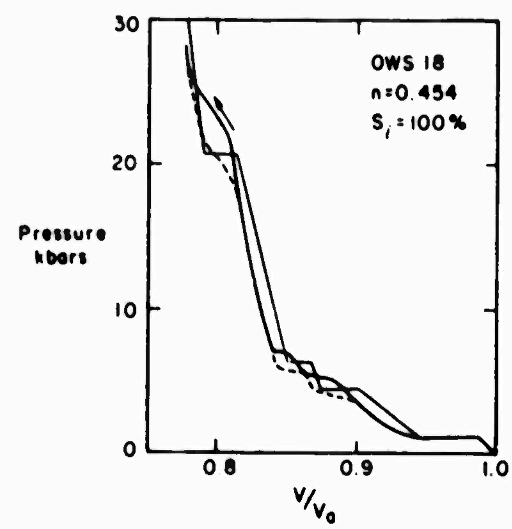

Figure 15. Isothermal compressibility of fully saturated Ottawa banding sand, specimen 18.

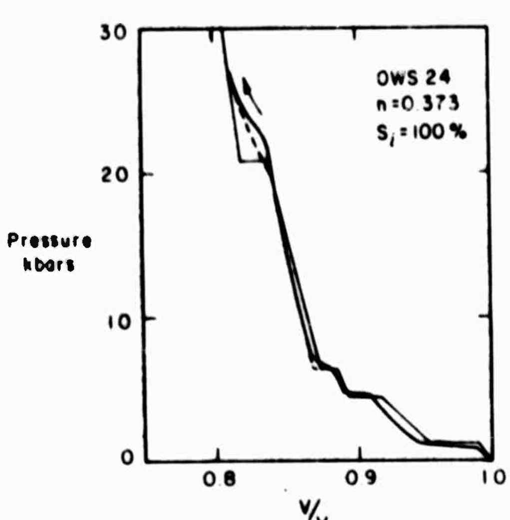

Figure 16. Isothermal compressibility of fully saturated Ottawa banding sand, specimen 24.

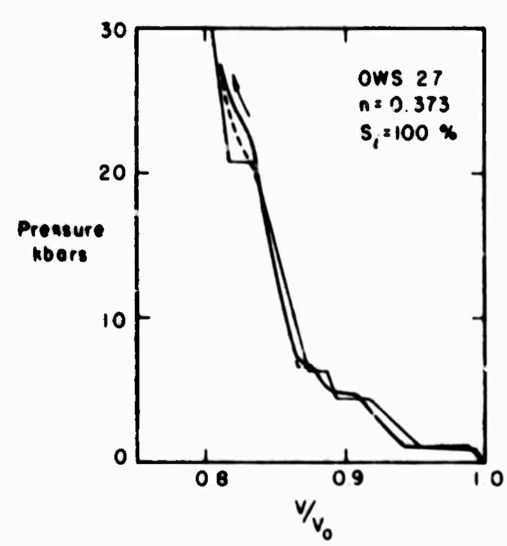

Figure 17. Isothermal compressibility of fully saturated Ottawa banding sand, specimen 27.

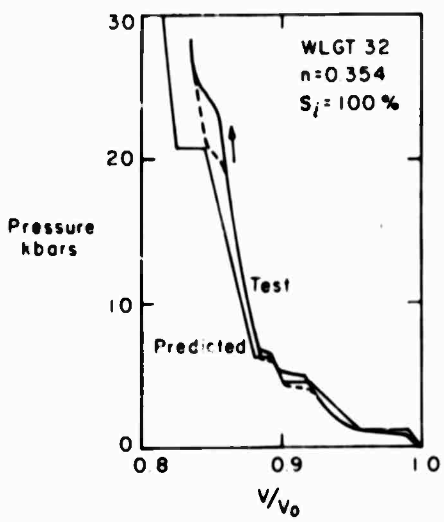

Figure 18. Isothermal compressibility of fully saturated West Lebanon glacial till, specimen 32.

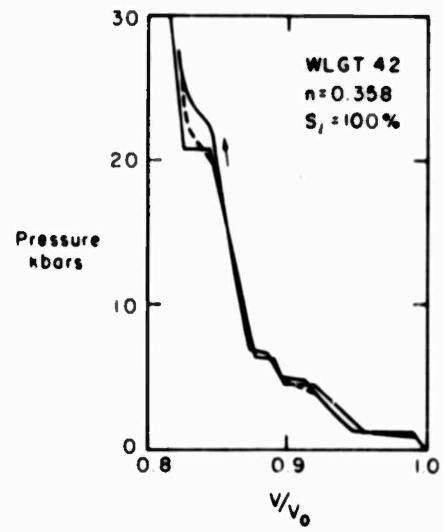

Figure 19. Isothermal compressibility of fully saturated West Lebanon glacial till, specimen 42.

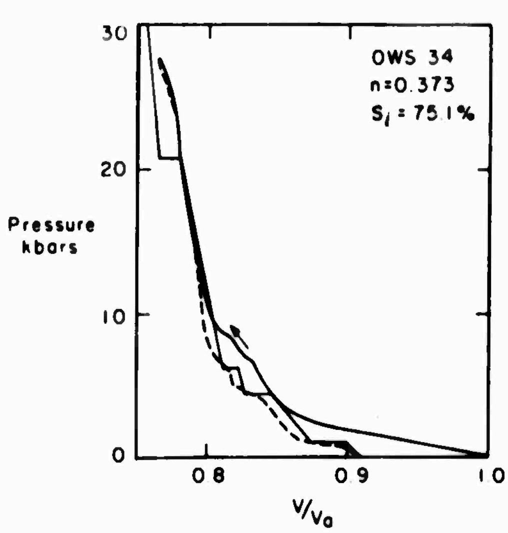

Figure 20. Isothermal compressibility of partially saturated Ottawa banding sand, specimen 34.

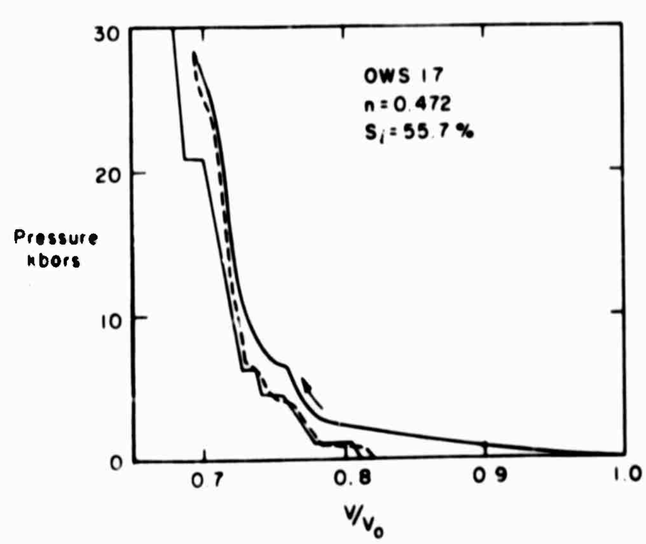

Figure 21. Isothermal compressibility of partially saturated Ottawa banding sand, specimen 17.

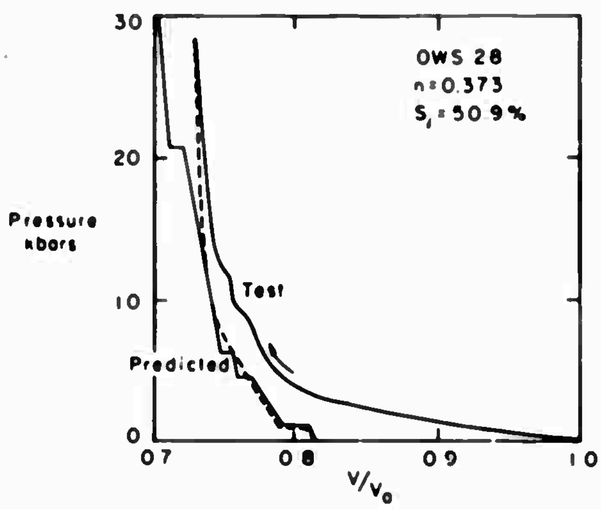

Figure 22. Isothermal compressibility of partially saturated Ottawa banding sand, specimen 28.

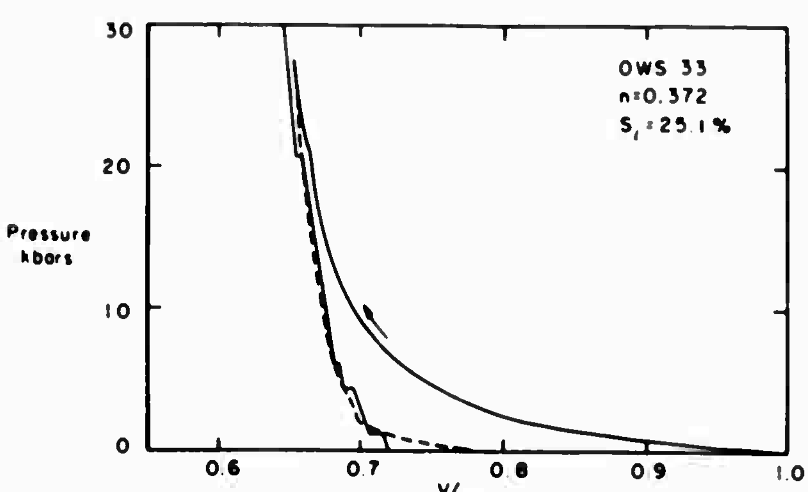

Figure 23. Isothermal compressibility of partially saturated Ottawa banding sand, specimen 33.

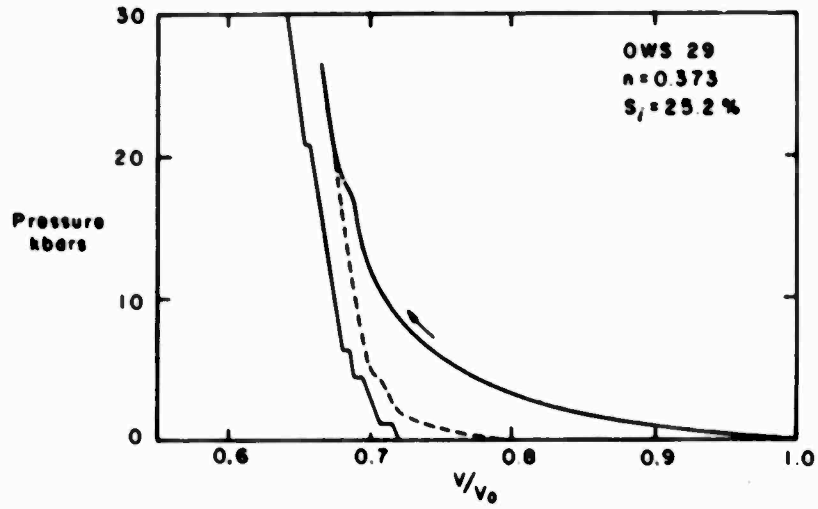

Figure 24. Isothermal compressibility of partially saturated Ottawa banding sand, specimen 29.

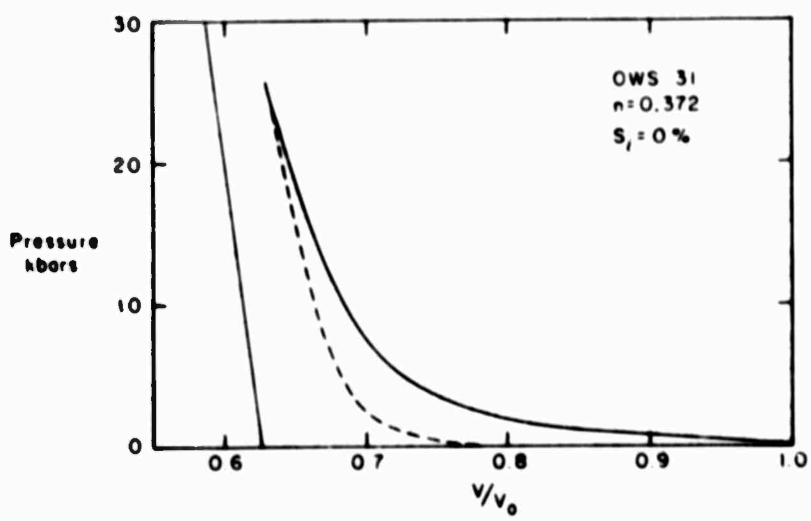

Figure 25. Isothermal compressibility of dry Ottawa banding sand, specimen 31.

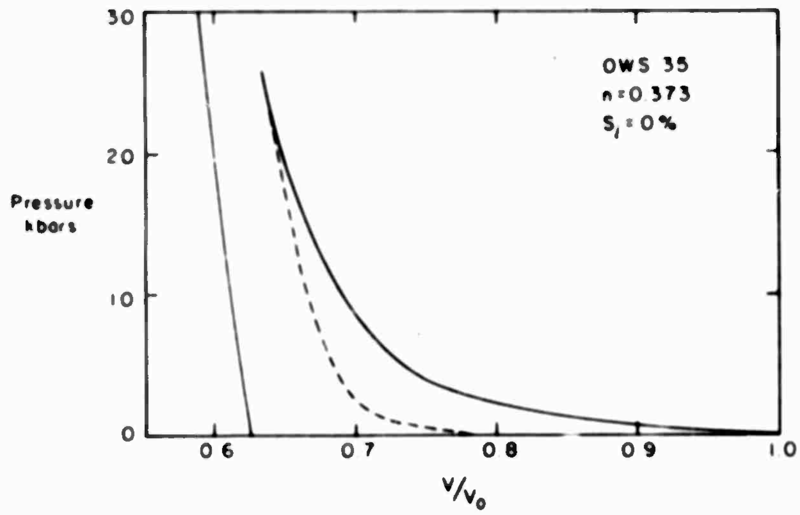

Figure 26. Isothermal compressibility of dry Ottawa banding sand, specimen 35.

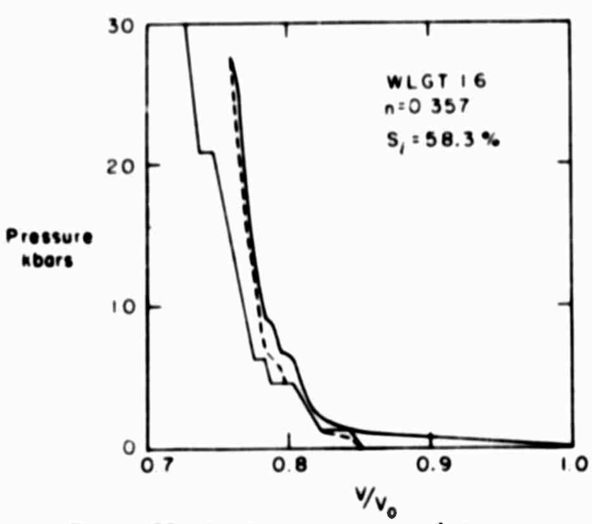

Figure 27. Isothermal compressibility of partially saturated West Lebanon glacial till, specimen 16.

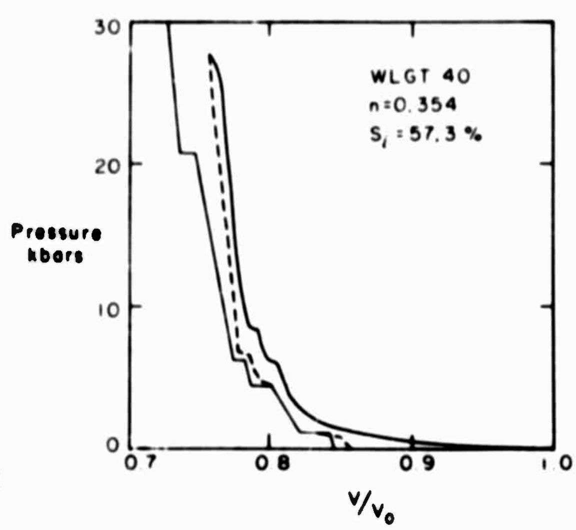

Figure 28. Isothermal compressibility of partially saturated West Lebanon glacial till, specimen 40.

and the Voigt average. The Reuss average B_r is given by:

$$B_r = V_a B_a + V_b B_b + V_c B_c + \ldots \tag{12}$$

where V_a, V_b, etc. are volume percentages of the minerals in the rock, and B_a, B_b, etc. are the volume compressibilities of the minerals. The Reuss average provides an upper bound. The lower bound, the Voigt average B_v is given by:

$$1/B_v = V_a/B_a + V_b/B_b + V_c/B_c + \ldots . \tag{13}$$

The Reuss averaging method assumes uniform distribution of stress throughout the matrix and neglects the difficulty in fitting the distorted grains together. The Voigt model assumes a uniform strain throughout the matrix and neglects the non-equilibrium stress conditions that exist. If discrepancies occurred between the predicted compressibilities given by eq 12 and 13 and the measured values, porosity or alterations of the minerals in the rock were listed as causes.

The prediction of the compressibility of frozen soil is analogous to that of rock. Fully and partially saturated frozen ground are discussed separately.

THE COMPRESSIBILITY OF FULLY SATURATED FROZEN GROUND

A saturated frozen ground can be considered as a rock made up of two components: ice and mineral particles. The compressibility of saturated frozen ground can be estimated by either eq 12 or 13 if we assume that the ice flows plastically. The problem is complicated by the phase transitions that ice undergoes when compressed to 30 kbars at -10C. This fact precludes the direct use of eq 12 or 13. A consequence of eq 12 is that the total volume change ΔV_s is the mere sum of the volume changes in the component materials, the mineral particles ΔV_m and the ice ΔV_i; i.e.

$$\Delta V_s = \Delta V_m + \Delta V_i. \tag{14}$$

With knowledge of ΔV_m and ΔV_i, ΔV_s can thus be computed at any pressure and temperature. Values for ΔV_m can be obtained from data given by Brace (1965), Stephens and Lilley (1966), and Stephens (1964).

A general equation for the compressibility of frozen ground, with porosity as the main parameter, can now be derived. Porosity n is defined as the ratio of the volume of voids V_v^0 to the total volume V_s^0 at atmospheric pressure:

$$n = V_v^0/V_s^0. \tag{15}$$

For a porous medium saturated with ice, eq 15 becomes:

$$n = V_i^0/V_s^0 \tag{16}$$

where V_i^0 is the volume of ice at atmospheric pressure.

ΔV_i at pressure P is given by:

$$\Delta V_i = nV_s^0\,(1 - v_i^P/v_i^0) \tag{17}$$

where v_i^P/v_i^0 is the value that can be obtained from Table VII, at any pressure. The volume of the mineral solids V_m^0 is:

$$V_m^0 = V_s^0 - V_i^0 \tag{18}$$

and ΔV_m is given by

$$\Delta V_m = (V_s^0 - V_i^0)(aP - bP^2) \tag{19}$$

where a and b are compressibility coefficients and P is pressure in kbars. Values for a range from 2.68×10^{-3} for quartz to 1.01×10^{-3} for augite (Brace, 1965). Values for b range from 24×10^{-6} for quartz to 3.9×10^{-6} for calcite.

The total volume change caused by pressure P is given by:

$$\Delta V_s = nV_s^0 \left(1 - v_i^p/v_i^0 \right) + \left(V_s^0 - V_i^0\right)\left(aP - bP^2\right). \tag{20}$$

The relative volume ratio V_s^p/V_s^0 is usually plotted versus P. Thus

$$V_s^p/V_s^0 = \Delta V_s/V_s^0 = 1 - n \; (1 - v_i^p/v_i^0) - (1 - n) + (aP + bP^2). \tag{21}$$

Figures 14-19 show the compressibilities of saturated frozen Ottawa banding sand and West Lebanon glacial till with the predicted compressibilities. The compressibilities for ice obtained from Bridgman's work are used for the prediction. Other than in the regions of the phase changes, the differences are subtle. The differences noted at the phase changes are of the same nature as those observed for pure ice. However, the ice VI-ice VIII transition appears to begin at a higher pressure than expected (22.5 kbars vs 20.8 kbars). This again may be the result of the time-dependent behavior of the reaction. But it may also be caused by a nonhomogeneous pressure distribution; i.e., the time is not sufficient for the pressure on the mineral component and that on the ice to equilibrate so the mineral component takes a higher pressure.

THE COMPRESSIBILITY OF PARTIALLY SATURATED FROZEN GROUND

By definition, unsaturated frozen ground consists of a mineral phase, a gas phase, and an ice phase. The degree of saturation S_i is defined as the ratio of the volume of the voids filled with ice V_i^0 and the total voids volume V_v^0. Thus

$$V_i^0 = S_i V_v^0. \tag{22}$$

V_i^0 can be expressed in terms of the total volume V_s^0 and the porosity n by

$$V_i^0 = S_i n V_s^0. \tag{23}$$

In an analogy with our analysis for saturated frozen ground, the changes in the volume of unsaturated frozen ground can be written as the sum of the true change in the volume of the mineral material ΔV_s, of the ice ΔV_i and of the air voids ΔV_a. Thus

$$\Delta V_s = \Delta V_m + \Delta V_i + \Delta V_a. \tag{24}$$

In a partially saturated soil, the volume of the air voids V_a^0 is given by

$$V_a^0 = \left(1 - S_i\right) V_v^0 = \left(1 - S_i\right) n \, V_s^0. \tag{25}$$

We will assume for now that all voids close with slight pressure. Then

$$\Delta V_a = V_a^0 = (1 - S_i) \, n \, V_s^0. \tag{26}$$

In an analogy with eq 17, the volume change of the ice at any pressure in an unsaturated frozen ground is given by

$$\Delta V_i = S_i\, n\, V_s^0 \;(1 - v_i^p / v_i^0) \tag{27}$$

and ΔV_m is given by

$$\Delta V_m = (V_s^0 - V_v^0)\;(aP + bP^2). \tag{28}$$

Hence

$$\Delta V_s = (1 - S_i)\, n\, V_s^0 + S_i\, n\, V_s^0 (1 - v_i^p/v_i^0) + (V_s^0 - V_v^0)(aP + bP^2). \tag{29}$$

and

$$V_s^p/V_s^0 = 1 - \Delta V_s/V_s^0 = 1 - (1 - S_i)\, n - S_i\, n\, (1 - v_i^p/v_i^0) - (1 - n)(aP + bP^2). \tag{30}$$

The isothermal compressibility of unsaturated frozen ground is thus a function of the degree of saturation with ice S_i the porosity n, and the isothermal compressibility of ice and mineral particles.

In Figures 20-28, the results for the compressibility of partially saturated Ottawa banding sand and West Lebanon glacial till are plotted with the predicted compressibility. The values used for a and b in eq 30 were 2.68×10^{-3} and 24×10^{-6}; P was in kbars. Specimens with various degrees of saturation were tested.

For the partially saturated ($S_i = 58\%$) West Lebanon glacial till (Fig 27 and 28) it appears that the air void closure occurred at some pressure below 2 kbars. The air void closure as observed is somewhat complicated and is partially obscured by the phase change that occurs at 1.11 kbars. The predicted compressibility is plotted for comparison. At the higher pressures there appears to be some deviation of the test results from the predicted values. Moreover, on the loading cycle the phase changes nucleate at a higher pressure than predicted. This occurrence indicates that complete air void closure has not taken place or, what is more likely, that the mineral component is subjected to a greater stress than the ice. This behavior is undoubtedly dependent upon the rate of compression.

The compressibilities for partially saturated Ottawa banding sand are plotted in Figures 20-26. Again the predicted values are shown for comparison. It appears that the air void closure is not obtained at 2 kbars. For 75% and 50% saturated specimens closure does not appear to occur until approximately 10 kbars. The phase changes are not well defined nor do they appear to be complete. Again, the phase changes nucleate at higher pressures than predicted. On the unloading curves the phase changes appear as predicted, although the rate dependence is still in evidence. The difference between the test results and the predicted values for the compressibilities of partially saturated sand is small (approximately 1% of the initial volume). This difference is well within the experimental accuracy.

It can be observed in the loading curves that a significant pressure is required to close the air voids. The prediction of the closure of the air voids as a function of pressure appears to be difficult.

The compressibility of rocks with small cracks or with spherical pores was investigated by Walsh (1965 a,b). He investigated analytically the elastic behavior of solids with cracks running through them. Important parameters are the shape and direction of the crack. Small differences in crack length with direction could lead to significant differences in linear compressibility. According to Walsh, the hydrostatic pressure necessary to close an elliptic cavity is

$$P = E\alpha \tag{31}$$

where E is Young's modulus and α is the ratio of minor to major radius of the cavity. A spherical cavity requires a larger pressure for closure. Equation 31 applies to a dry homogeneous rock, or to a dry nonhomogeneous rock if E is the Young's modulus of the weakest material. Equation 31 also assumes that the cavity is closed by elastic deformation. If the crack is closed by plastic flow or by brittle failure, eq 31 does not apply.

On the other hand, partially saturated frozen ground consists of ice and an unconsolidated mineral matrix. The first reduction in air void volume would occur not by elastic deformation or by plastic flow but by rearrangement of the mineral particles. This would be followed or accompanied by crushing of the individual particles. The extent of the rearrangement and the crushing would be governed by the amount of ice present. As the mineral particles are being rearranged and crushed, the ice would flow plastically. At some pressure the ice would completely fill the voids and be subjected to the same overall pressure as the particles. The compressibility then would be governed by the deformation of the mineral particles and the plastic deformation of the ice.

The pressure at which the air voids close is influenced by the degree of saturation with ice. The air voids in soils with a high degree of saturation would close at a relatively low pressure while those with a low degree of saturation would require a higher pressure for air void closure. Moreover, the rearrangement and crushing may be expected to be more efficient for a wet soil than for a dry soil.

The Ottawa sand specimen 33 (Fig. 23), with a 25% saturation, exhibits a somewhat different behavior from that of the specimens with higher degrees of saturation. Closure does not appear to occur until a pressure of approximately 20 kbars has been reached. Upon unloading, the test data follow the predicted data down to a pressure of approximately 1 kbar. The phase changes are not well defined. This would be expected because of the small volume of ice present. However, at approximately 1 kbar, the test data leave the predicted values and the specimen appears to expand elastically. Figures 25 and 26 show that the dry Ottawa sand specimens have the same elastic expansion for the low-pressure release curve. In fact, the dry and 25% saturated specimens release to approximately the same relative volume (0.78). This relative volume is the smallest volume regardless of the degree of saturation to which Ottawa banding sand can be compressed under the test conditions.

The Ottawa banding sand compressibility curves look much like those reported for dry Monterey sand by Stephens and Lilley (1966). Complete closure of the voids is not obtained and the mineral particles deform elastically.

To test the validity of the methods used in reducing the raw data for the partially saturated soils, the first and second compressibilities were calculated for a fully saturated sand. The results of this comparison (Fig. 29) indicate that the methods used to reduce the data from the first compression are valid. However, the phase transition of ice I to water is somewhat obscured and the subsequent phase transitions occur at somewhat high pressures than expected.

The results of three compression cycles on dry Ottawa banding sand are illustrated in Figure 30. This figure shows that the voids undergo maximum closure during the first compression. The first release curve and the additional compression cycles follow nearly the same path. Thus, it appears that the working of the mineral particles and the subsequent breakdown do not result in a further change in compressibility.

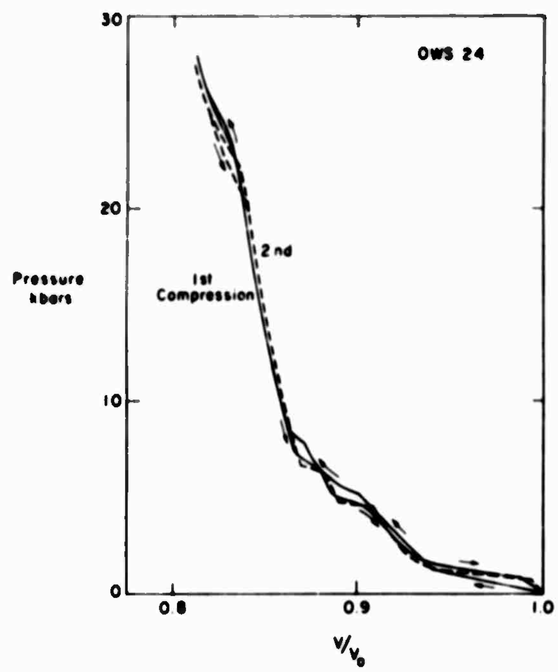

Figure 29. First and second compressibilities of fully saturated Ottawa banding sand, specimen 24.

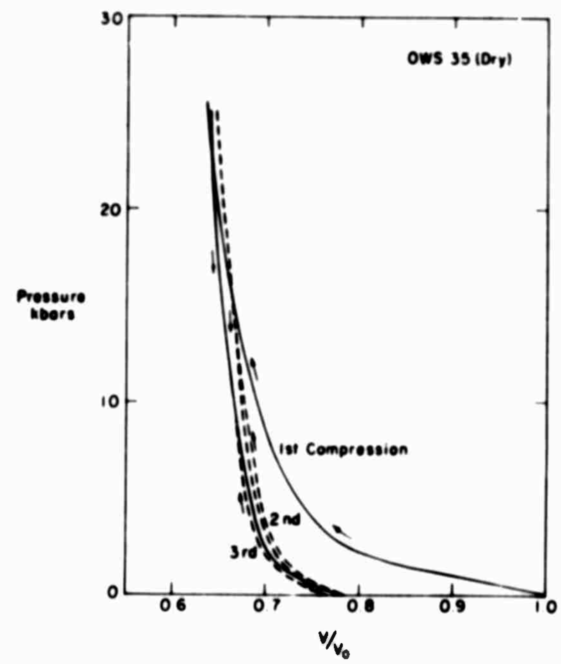

Figure 30. First, second and third compressibilities of dry Ottawa banding sand, specimen 35.

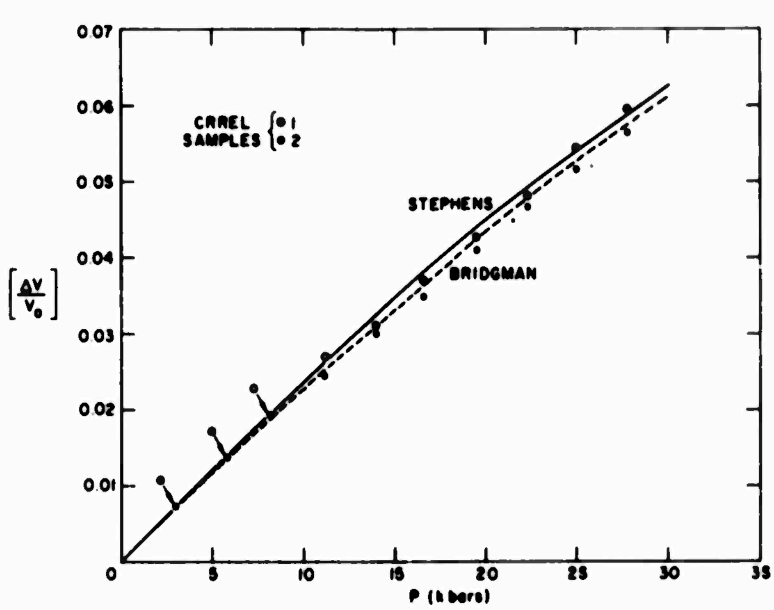

Figure 31. The isothermal compressibility of indium.

The isothermal compressibility of indium was determined as an additional check on the accuracy of our procedures and equipment. The procedures followed were identical to those used for the compressibility of the frozen sand, frozen silt, and ice. The compressibility of indium was compared with that of gold. The results are given in Figure 31. Results obtained by Bridgman (1935) and Stephens (1967) are shown for comparison.

CONCLUSIONS

The compressibility of frozen soil is readily predicted from the knowledge of material properties such as the degree of saturation with ice, the porosity, and the compressibilities of the ice and mineral components. The behavior of the phase transitions for partially saturated frozen soils is somewhat obscured by the rearrangement and crushing of the mineral particles. Materials with no ice or a low degree of saturation demonstrate elastic rebound on the release leg of the compression cycle. Apparently there is a maximum dry density to which a particular soil can be compressed, and this density is somewhat less than that of the voidless mineral parent.

The compressibility of ice is as predicted by Bridgman (1911, 1937). However, time-dependent behavior is demonstrated for the phase transitions. Complete phase transitions were not observed at constant pressure.

The compressibilities in the low-pressure region (below 2 kbars) were not well defined. This is primarily a result of the test method. A technique employing a liquid cell in the low-pressure region is being pursued and the results will be reported later.

LITERATURE CITED

Adams, L.H. and Williamson, E.D. (1923) On the compressibility of minerals and rocks at high pressures. *Journal of the Franklin Institute*, vol. 195, p. 475-525.

Bassett, W.A.; Takahashi, Taro; Mao, Ho-Kwang and Weaver, J. Scott. (1968) Pressure-induced phase transformation in NaCl. *Journal of Applied Physics*., vol. 39, no. 1.

Brace, W.F. (1965) Some new measurements of linear compressibility of rocks. *Journal of Geophysical Research*, vol. 70, no. 2, p. 391-397.

Bridgman, P.W. (1911) Water in the liquid and five solid forms, under pressure. *Proceedings of the American Academy of Arts and Sciences*, vol. 47, p. 441-558.

__________ (1912) Thermodynamic properties of liquid water to 80° and 12,000 kgm. *Proceedings of the American Academy of Arts and Sciences*, vol. 48, p. 309-362

__________ (1914) High pressures and five kinds of ice. *Journal of the Franklin Institute*, vol. 177, p. 315-332.

__________ (1937) The phase diagram of water to 45,000 kg/cm^2. *Journal of Chemical Physics*, vol. 5, p. 964-966.

__________ (1940) The compression of 46 substances to 50,000 kg/cm^2. *American Academy of Arts and Sciences*, vol. 74, p. 21-51.

__________ (1964) *Collected experimental papers*. Cambridge, Mass. Harvard University Press, 7 vols.

LITERATURE CITED (Cont'd)

Brown, A.J. and Whalley, E. (1966) Preliminary investigation of the phase boundaries between ice VI and VII and ice VIII. *Journal of Chemical Physics*, vol. 45, p. 4360-4361.

Brown, Wayne; DeVries, K.L. and Smith, J.L. (1967) Properties of rock tested in one-dimensional compression. Air Force Weapons Laboratory, AFWL-TR-66-124.

Paulding, B.W.; Cornish, R.H.; Abbott, B.W. and Finlayson, L.A. (1965) Behavior of rocks and soils under high pressure. Air Force Weapons Laboratory, AFWL-TR-65-51.

Stephens, D.R. (1934) The hydrostatic compression of eight rocks. *Journal of Geophysical Research*, vol. 69, no. 14, p. 2967-2977.

__________ and Lilley, E.M. (1966) Static PV curves of cracked and consolidated earth materials to 40 kb. University of California, Lawrence Radiation Laboratory, UCRL-14711.

__________ and Lilley, E.M. (1967) Procedure for pressure-volume runs on rocks. University of California, Lawrence Radiation Laboratory, UCID-15070.

Walsh, J.B. (1965a) The effect of cracks on the compressibility of rock. *Journal of Geophysical Research*, vol. 70, no. 2, p. 381-389.

Walsh, J.B. (1965b) The effect of cracks on the uniaxial elastic compression of rocks. *Journal of Geophysical Research*, vol. 70, no. 2, p. 399-411.

Whalley, E.; Davidson, D.W. and Heath, J.B.R. (1966) Dielectric properties of ice VII, ice VIII: a new phase of ice. *Journal of Chemical Physics*, vol. 45, no. 11, p. 3976-3982.

Wilson, G.J.; Chan, R.K.; Davidson, D.W. and Whalley E. (1965) Dielectric properties of ices II, III, V, and VI. *Journal of Chemical Physics*, vol. 43, no. 7, p. 2384-2391.

Table AI. Isothermal compressibility of polycrystalline ice specimen 11.

Pressure kbars	Volume cm^3	Relative Volume
0.00	2.6500	1.0000
0.75	2.6152	0.9869
1.00	2.5100	0.9472
1.25	2.3309	0.8796
1.43	2.2666	0.8553
2.76	2.1711	0.8193
3.76	2.1197	0.7999
4.51	2.0796	0.7848
4.76	2.0289	0.7656
5.51	1.9528	0.7369
6.52	1.8953	0.7152
6.77	1.7983	0.6786
7.52	1.7914	0.6760
10.03	1.7680	0.6672
12.53	1.7478	0.6595
17.54	1.7190	0.6487
19.05	1.7068	0.6441
19.80	1.7017	0.6422
20.30	1.6974	0.6405
21.05	1.6871	0.6367
21.81	1.5944	0.6017
22.56	1.5476	0.5840
24.31	1.5323	0.5782
27.57	1.5243	0.5752
30.08	1.5156	0.5719
22.56	1.5344	0.5790
21.81	1.5351	0.5793
21.05	1.5389	0.5807
20.30	1.5656	0.5908
19.80	1.6638	0.6279
19.05	1.7068	0.6441
17.54	1.7190	0.6487
12.53	1.7478	0.6595
10.03	1.7680	0.6672
7.52	1.7914	0.6760
6.76	1.7983	0.6786
6.52	1.8047	0.6810
5.51	1.9182	0.7238
4.76	1.9350	0.7302
4.51	1.9445	0.7338
3.76	2.1197	0.7999
2.76	2.1711	0.8193
1.43	2.2666	0.8553
1.25	2.3309	0.8796
1.00	2.5110	0.9472
0.75	2.6152	0.9869
0.00	2.6500	1.0000

Table AII. Isothermal compressibility of polycrystalline ice specimen 43.

Pressure kbars	Volume cm^3	Relative Volume
0.00	2.7640	1.0000
0.78	2.7384	0.9907
1.25	2.4495	0.8862
1.38	2.4047	0.8700
1.68	2.3630	0.8549
2.51	2.2846	0.8266
3.31	2.2284	0.8062
4.79	2.1504	0.7780
5.26	2.0364	0.7368
6.27	1.9387	0.7014
7.52	1.8942	0.6853
10.03	1.8487	0.6689
12.53	1.8259	0.6606
15.04	1.8073	0.6539
17.54	1.7917	0.6482
19.30	1.7813	0.6445
20.68	1.7726	0.6413
21.03	1.7182	0.6216
21.30	1.6492	0.5967
21.91	1.6048	0.5806
22.56	1.6032	0.5800
25.06	1.5931	0.5764
27.57	1.5874	0.5743
29.02	1.5805	0.5718
20.45	1.6131	0.5836
20.05	1.7150	0.6205
19.30	1.7590	0.6364
17.54	1.7917	0.6482
15.04	1.8073	0.6539
12.53	1.8259	0.6606
10.03	1.8437	0.6679
7.52	1.8728	0.6776
6.69	1.8837	0.6815
6.64	1.9800	0.7164
4.84	2.0048	0.7253
3.76	2.1490	0.7775
3.31	2.2284	0.8062
2.51	2.2846	0.8266
1.68	2.3630	0.8549
1.33	2.4047	0.8700
1.25	2.4495	0.8862
0.78	2.7384	0.9907
0.00	2.7640	1.0000

Table AIII. Isothermal compressibility of polycrystalline ice specimen 44.

Pressure kbars	Volume cm^3	Relative Volume
0.00	2.8880	1.0000
1.00	2.8632	0.9931
1.50	2.5387	0.8806
1.88	2.4361	0.8450
2.38	2.3932	0.8301
3.76	2.3107	0.8015
5.01	2.2529	0.7814
5.14	2.2113	0.7670
5.64	2.1666	0.7515
6.24	2.1354	0.7407
6.39	2.0349	0.7058
6.64	1.9977	0.6929
7.52	1.9595	0.6797
8.15	1.9456	0.6749
10.03	1.9259	0.6680
12.53	1.9047	0.6607
15.04	1.8868	0.6545
17.54	1.8676	0.6478
20.13	1.8534	0.6429
21.66	1.6744	0.5808
25.06	1.6651	0.5776
27.57	1.6526	0.5732
28.32	1.6519	0.5730
27.57	1.6526	0.5732
25.06	1.6651	0.5776
21.66	1.6744	0.5808
20.13	1.8534	0.6429
17.54	1.8676	0.6478
15.04	1.8868	0.6545
12.53	1.9047	0.6607
10.03	1.9259	0.6680
8.15	1.9456	0.6749
7.52	1.9595	0.6797
6.64	1.9977	0.6929
6.49	1.9706	0.6835
6.37	2.0579	0.7138
4.59	2.0859	0.7235
3.76	2.1871	0.7586
3.13	2.3101	0.8013
2.38	2.4060	0.8345
1.88	2.4515	0.8503
1.30	2.4987	0.8667
1.00	2.6734	0.9273
0.50	2.7926	0.9686
0.00	2.8652	0.9938

Table AIV. Isothermal compressibility of Ottawa banding sand specimen 31.

n = 0.372 S_1 = 0%

Pressure kbars	Volume cm^3	Relative Volume
0.00	2.7220	1.0000
1.25	2.3093	0.8484
1.75	2.1962	0.8068
2.51	2.1154	0.7772
3.76	2.0309	0.7461
5.01	1.9749	0.7255
6.27	1.9337	0.7104
7.52	1.9024	0.6989
10.03	1.8596	0.6832
12.53	1.8289	0.6719
15.04	1.7993	0.6612
17.54	1.7727	0.6512
20.05	1.7485	0.6423
22.56	1.7309	0.6359
25.69	1.7094	0.6280
22.56	1.7299	0.6355
17.54	1.7532	0.6459
15.04	1.7729	0.6513
12.53	1.7896	0.6575
10.03	1.8031	0.6624
7.52	1.8285	0.6718
5.01	1.8548	0.6814
3.76	1.8750	0.6888
2.51	1.9038	0.6994
1.25	1.9524	0.7173
0.50	2.0224	0.7430
0.00	2.1007	0.7717

Table AV. Isothermal compressibility of Ottawa banding sand specimen 35.

n = 0.373 S_1 = 0%

COMPRESSION No. 1			COMPRESSION No. 2			COMPRESSION No. 3		
Press. kbars	Vol. cm^3	Rel. Vol.	Press. kbars	Vol. cm^3	Rel. Vol.	Press. kbars	Vol. cm^3	Rel. Vol.
0.00	2.7220	1.0000	0.00	2.1353	0.7845	0.00	2.0808	0.7644
0.63	2.5539	0.9382	0.25	2.0834	0.7654	0.58	2.0019	0.7354
1.25	2.3447	0.8614	0.50	2.0518	0.7538	0.95	1.9633	0.7213
1.88	2.2130	0.8130	1.25	1.9901	0.7311	1.50	1.9264	0.7077
2.51	2.1372	0.7852	2.51	1.9378	0.7119	2.46	1.8929	0.6954
3.76	2.0466	0.7519	5.01	1.8875	0.6934	3.88	1.8637	0.6847
5.01	1.9933	0.7323	7.52	1.8629	0.6844	5.01	1.8485	0.6791
7.52	1.9243	0.7070	10.03	1.8444	0.6776	7.52	1.8273	0.6713
10.03	1.8742	0.6886	12.53	1.8266	0.6711	10.03	1.8109	0.6653
12.53	1.8366	0.6747	15.04	1.8116	0.6655	12.53	1.7963	0.6599
15.04	1.8086	0.6642	17.54	1.7990	0.6609	15.04	1.7813	0.6544
17.54	1.7839	0.6554	20.05	1.7865	0.6563	17.54	1.7694	0.6500
20.05	1.7661	0.6488	22.56	1.7726	0.6512	20.05	1.7589	0.6462
22.56	1.7445	0.6409	25.06	1.7590	0.6462	22.56	1.7484	0.6423
25.06	1.7287	0.6351	17.54	1.7982	0.6606	25.06	1.7381	0.6385
25.69	1.7260	0.6341	15.04	1.8091	0.6646	22.56	1.7484	0.6423
25.06	1.7287	0.6351	12.53	1.8208	0.6689	20.05	1.7589	0.6462
22.56	1.7445	0.6409	10.03	1.8352	0.6742	17.54	1.7694	0.6500
20.05	1.7569	0.6455	7.52	1.8529	0.6807	15.04	1.7813	0.6544
17.54	1.7500	0.6429	5.01	1.8783	0.6901	12.53	1.7963	0.6599
15.04	1.7795	0.6537	2.51	1.9219	0.7061	10.03	1.8109	0.6653
12.53	1.7949	0.6594	1.25	1.9708	0.7240	7.52	1.8273	0.6713
10.03	1.8115	0.6655	0.50	2.0249	0.7439	5.01	1.8485	0.6719
7.52	1.8290	0.6719	0.25	2.0499	0.7531	3.89	1.8637	0.6847
5.01	1.8568	0.6821	0.00	2.0808	0.7644	2.46	1.8929	0.6954
2.51	1.9043	0.6996				1.50	1.9264	0.7077
1.25	1.9569	0.7189				0.95	1.9633	0.7213
0.63	2.0240	0.7436				0.58	2.0019	0.7354
0.00	2.1263	0.7819				0.00	2.0808	0.7644

Table AVI. Isothermal compressibility of Ottawa banding sand specimen 29.

n = 0.373 S_i = 25.2%

Pressure kbars	Volume cm³	Relative Volume
0.00	2.7220	1.0000
0.50	2.5746	0.9453
1.25	2.4056	0.8833
2.51	2.2321	0.8200
3.76	2.1265	0.7812
5.01	2.0634	0.7580
6.27	2.0209	0.7424
7.52	1.9859	0.7296
10.03	1.9360	0.7112
12.53	1.8963	0.6969
15.04	1.8787	0.6902
17.54	1.8635	0.6846
[illegible]	1.8475	0.6787
20.05	1.8405	0.676[illegible]
22.55	1.8240	0.6701
25.06	1.8146	0.6667
26.34	1.8100	0.6650
25.06	1.8146	0.6667
22.56	1.8240	0.6701
20.05	1.8351	0.6742
17.54	1.8453	0.67[illegible]
15.04	1.8553	0.6[illegible]16
12.53	1.8651	0.6852
10.03	1.8771	0.6896
[illegible]	1.8899	0.6943
5.01	1.9059	0.7002
4.26	1.9229	0.7064
[illegible]	1.9340	0.710[illegible]
[illegible]	1.9550	[illegible]
1.25	1.9910	0.7322
0.50	2.0849	0.7556
0.00	2.1[illegible]	0.7901

Table AVII. Isothermal compressibility of Ottawa banding sand specimen 33.

n = 0.372 S_i = 25.1%

Pressure kbars	Volume cm³	Relative Volume
0.00	2.7220	1.0000
0.25	2.6776	0.9837
0.50	2.5713	0.9446
1.25	2.3609	0.8673
2.51	2.1791	0.8006
5.01	2.0210	0.7425
7.52	1.9425	0.7136
10.03	1.8926	0.6953
12.53	1.8552	0.6816
15.04	1.8351	0.6742
17.54	1.8227	0.6696
20.05	1.8083	0.6643
22.56	1.7934	0.6591
25.06	1.7827	0.6549
27.57	1.7723	0.6513
25.06	1.7820	0.6547
22.56	1.7875	0.6567
20.05	1.7909	0.6580
17.54	1.7933	0.6605
15.04	1.8033	0.6643
12.53	1.8203	0.6687
10.03	1.8302	0.6724
7.52	1.8426	0.6769
5.01	1.8619	0.6840
3.76	1.8846	0.6924
3.26	1.8895	0.6941
2.50	1.8994	0.6973
2.26	1.9012	0.6984
1.25	1.9550	0.7182
0.50	2.0309	0.7461
0.00	2.1417	0.7894

Table AVIII. Isothermal compressibility of Ottawa banding sand specimen 28.

n = 0.373 S_i = 50.9%

Pressure kbars	Volume cm³	Relative Volume
0.00	2.7220	1.0000
0.25	2.6563	0.9759
0.50	2.6099	0.9588
0.75	2.5668	0.9430
1.00	2.5196	0.9257
1.25	2.4319	0.9113
1.75	2.4050	0.8835
2.51	2.3125	0.8496
3.76	2.1877	0.8037
5.01	2.1319	0.7832
7.52	2.1001	0.7715
8.77	2.0851	0.7660
10.03	2.0585	0.7562
11.73	2.0477	0.7523
12.53	2.0366	0.7482
15.04	2.0164	0.7408
17.54	2.0101	0.7385
20.05	2.0030	0.7359
22.56	1.9939	0.7325
25.06	1.9905	0.7313
28.32	1.9822	0.7282
25.06	1.9856	0.7295
22.56	1.9873	0.7301
20.05	1.9898	0.7310
17.54	1.9928	0.7321
15.04	2.0000	0.7347
12.53	2.0099	0.7369
10.03	2.0153	0.7406
7.52	2.0349	0.7476
6.27	2.0475	0.7522
4.39	2.0845	0.7658
1.25	2.1445	0.7879
0.91	2.1986	0.8077
0.00	2.2164	0.8143

Table AIX. Isothermal compressibility of Ottawa banding sand specimen 17.

n = 0.427 S_i = 55.7%

Pressure kbars	Volume cm^3	Relative Volume
0.00	2.7110	1.0000
0.25	2.5576	0.9434
0.50	2.4941	0.9200
0.75	2.4400	0.9000
1.00	2.3885	0.8810
1.25	2.3480	0.8661
1.50	2.3110	0.8525
1.75	2.2723	0.8382
2.00	2.2341	0.8241
2.26	2.1949	0.8096
2.51	2.1538	0.7945
2.76	2.1297	0.7856
3.26	2.1071	0.7772
3.76	2.0986	0.7741
6.44	2.0538	0.7576
6.52	2.0463	0.7548
6.77	2.0329	0.7499
7.52	2.0152	0.7433
8.77	1.9955	0.7361
10.03	1.9783	0.7297
12.53	1.9629	0.7240
15.04	1.9523	0.7202
17.54	1.9431	0.7167
20.05	1.9363	0.7143
25.06	1.9137	0.7059
26.32	1.9047	0.7026
28.27	1.8794	0.6932
25.06	1.8989	0.7004
22.56	1.9168	0.7071
20.05	1.9286	0.7114
17.54	1.9366	0.7143
15.04	1.9454	0.7176
12.53	1.9539	0.7207
10.03	1.9639	0.7244
7.52	1.9765	0.7291
6.89	1.9806	0.7306
6.27	2.0016	0.7383
5.01	2.0184	0.7445
4.66	2.0252	0.7470
4.26	2.0535	0.7575
3.76	2.0687	0.7631
2.51	2.0912	0.7714
1.05	2.1251	0.7839
0.80	2.2086	0.8147
0.00	2.2186	0.8184

Table AX. Isothermal compressibility of Ottawa banding sand specimen 34.

n = 0.373 S_i = 75.1%

Pressure kbars	Volume cm^3	Relative Volume
0.00	2.7220	1.0000
1.25	2.5790	0.9475
2.00	2.4432	0.8976
2.51	2.3845	0.8760
3.01	2.3416	0.8602
3.76	2.3140	0.8501
5.01	2.2900	0.8413
6.77	2.2644	0.8319
7.02	2.2175	0.8161
8.77	2.2136	0.8132
10.03	2.1853	0.8025
12.53	2.1653	0.7955
15.04	2.1511	0.7903
17.54	2.1398	0.7861
20.05	2.1298	0.7824
22.56	2.1210	0.7792
25.06	2.1114	0.7757
26.32	2.0990	0.7711
27.32	2.0820	0.7649
26.32	2.0920	0.7685
25.06	2.1073	0.7742
23.31	2.1222	0.7796
22.56	2.1210	0.7792
20.05	2.1298	0.7824
17.54	2.1387	0.7857
15.04	2.1471	0.7888
12.53	2.1563	0.7922
10.03	2.1684	0.7966
7.52	2.1831	0.8020
7.02	2.1922	0.8054
6.52	2.2096	0.8117
6.02	2.2203	0.8157
5.01	2.2317	0.8199
4.06	2.2891	0.8410
2.51	2.3188	0.8519
1.20	2.3567	0.8658
0.30	2.4457	0.8985
0.00	2.4674	0.9065

Table AXI. Isothermal compressibility of Ottawa banding sand specimen 1.

n = 0.378 S_i = 100%

Pressure kbars	Volume cm^3	Relative Volume
0.00	2.6070	1.0000
1.00	2.5781	0.9889
1.18	2.4487	0.9393
2.51	2.4085	0.9239
4.69	2.3663	0.9077
4.79	2.3089	0.8856
6.34	2.2887	0.8779
6.64	2.2560	0.8654
7.52	2.2476	0.8621
10.03	2.2304	0.8555
12.53	2.2156	0.8499
15.04	2.2029	0.8450
17.54	2.1900	0.8401
18.80	2.1838	0.8377
21.30	2.1703	0.8325
22.56	2.1527	0.8258
23.81	2.1330	0.8182
25.06	2.1205	0.8134
26.32	2.1120	0.8101
27.32	2.1011	0.8060
25.06	2.1188	0.8123
22.56	2.1310	0.8174
21.30	2.1469	0.8235
20.05	2.1716	0.8330
18.80	2.1838	0.8377
17.54	2.1900	0.8401
15.04	2.2029	0.8450
12.53	2.2156	0.8499
10.03	2.2304	0.8555
7.52	2.2476	0.8621
6.64	2.2560	0.8654
6.34	2.2887	0.8779
4.79	2.3089	0.8856
4.69	2.3663	0.9077
2.51	2.4085	0.9239
1.18	2.4487	0.9393
1.00	2.5781	0.9889
0.00	2.6070	1.0000

Table AXII. Isothermal compressibility of Ottawa banding sand specimen 18.

n = 0.454 S_i = 100%

Pressure kbars	Volume cm³	Relative Volume
0.00	2.7110	1.0000
0.25	2.6979	0.9952
1.00	2.6790	0.9882
1.25	2.5375	0.9360
1.50	2.5134	0.9271
3.76	2.4370	0.8989
5.01	2.3968	0.8841
5.51	2.3375	0.8622
6.77	2.3168	0.8546
7.27	2.2787	0.8405
10.03	2.2573	0.8326
18.05	2.2092	0.8149
20.05	2.2037	0.8129
21.30	2.1972	0.8105
22.56	2.1845	0.8058
23.81	2.1548	0.7948
25.06	2.1302	0.7857
27.57	2.1065	0.7770
28.32	2.1053	0.7766
27.57	2.1065	0.7770
22.56	2.1306	0.7859
21.30	2.1416	0.7900
20.05	2.1726	0.8014
18.80	2.2006	0.8117
18.05	2.2092	0.8149
10.03	2.2578	0.8328
7.27	2.2787	0.8405
6.02	2.2893	0.8444
5.76	2.3312	0.8599
5.51	2.3375	0.8622
4.51	2.3518	0.8675
3.76	2.4370	0.8989
1.50	2.5134	0.9271
1.25	2.5375	0.9360
1.00	2.6790	0.9882
0.25	2.6979	0.9952
0.00	2.7110	1.0000

Table AXIII. Isothermal compressibility of Ottawa banding sand specimen 24.

n = 0.373 S_i = 100%

COMPRESSION No. 1

Press. kbars	Vol. cm³	Rel. Vol.
0.00	2.7150	1.0000
0.65	2.6537	0.9749
1.00	2.5838	0.9511
1.25	2.5623	0.9413
1.75	2.5473	0.9358
2.26	2.5295	0.9293
2.51	2.5224	0.9267
3.76	2.4931	0.9159
5.19	2.4518	0.9007
5.51	2.4282	0.8921
6.01	2.4078	0.8846
7.77	2.3737	0.8720
8.27	2.3571	0.8659
8.77	2.3465	0.8621
10.03	2.3366	0.8584
12.53	2.3208	0.8526
15.04	2.3055	0.8470
17.54	2.2941	0.8428
20.05	2.2808	0.8379
22.56	2.2699	0.8339
23.81	2.2616	0.8308
25.06	2.2437	0.8243
26.32	2.2239	0.8170
27.97	2.2121	0.8127
25.06	2.2383	0.8223
23.81	2.2590	0.8299
22.56	2.2687	0.8335
20.05	2.2808	0.8379
17.54	2.2941	0.8428
15.04	2.3055	0.8470
12.53	2.3208	0.8526
10.03	2.3366	0.8584
8.77	2.3432	0.8608
7.52	2.3533	0.8645
7.02	2.3638	0.8684
6.52	2.3965	0.8804
6.01	2.4021	0.8825
5.51	2.4069	0.8842
5.01	2.4157	0.8875
4.51	2.4641	0.9053
2.26	2.5314	0.9300
1.75	2.5494	0.9366
1.50	2.5635	0.9413
1.25	2.6109	0.9592
1.00	2.6584	0.9766
0.75	2.6894	0.9880
0.00	2.7150	1.0000

COMPRESSION No. 2

Press. kbars	Vol. cm³	Rel. Vol.
0.00	2.7150	1.0000
0.25	2.7090	0.9978
0.50	2.7033	0.9957
0.73	2.6983	0.9939
1.25	2.5631	0.9440
2.51	2.5209	0.9285
3.76	2.4880	0.9164
4.51	2.4682	0.9091
4.79	2.4162	0.8900
6.27	2.3941	0.8818
6.52	2.3816	0.8772
6.77	2.3673	0.8720
7.02	2.3612	0.8697
7.52	2.3537	0.8669
10.03	2.3365	0.8606
12.53	2.3204	0.8546
15.04	2.3085	0.8503
17.54	2.2959	0.8456
20.05	2.2821	0.8406
21.30	2.2779	0.8390
22.56	2.2660	0.8346
23.81	2.2431	0.8262
25.06	2.2237	0.8191
26.32	2.2122	0.8143
27.27	2.2029	0.8114
26.32	2.2122	0.8143
23.81	2.2357	0.8235
22.56	2.2433	0.8263
21.30	2.2664	0.8348
20.05	2.2821	0.8406
17.54	2.2959	0.8456
15.04	2.3085	0.8503
12.53	2.3204	0.8546
10.03	2.3365	0.8606
7.52	2.3537	0.8669
7.02	2.3612	0.8697
6.77	2.3600	0.8692
6.52	2.3816	0.8772
6.27	2.3941	0.8818
4.79	2.4162	0.8900
4.51	2.4682	0.9091
3.76	2.4880	0.9164
2.51	2.5209	0.9285
1.25	2.5631	0.9440
0.73	2.6983	0.9939
0.50	2.7033	0.9957
0.25	2.7090	0.9987
0.00	2.7150	1.0000

Table AXIV. Isothermal compressibility of Ottawa banding sand specimen 27.

n = 0.373 S_i = 100%

Pressure kbars	Volume cm^3	Relative Volume
0.00	2.7220	1.0000
0.90	2.7030	0.9930
1.13	2.5665	0.9429
2.51	2.5229	0.9268
4.56	2.4751	0.9093
5.01	2.4162	0.8877
6.62	2.3886	0.8775
6.77	2.3836	0.8757
7.02	2.3630	0.8681
7.52	2.3502	0.8634
10.03	2.3352	0.8579
12.53	2.3197	0.8522
15.04	2.3059	0.8471
17.54	2.2936	0.8426
20.05	2.2817	0.8382
21.30	2.2760	0.8361
22.56	2.2661	0.8325
23.81	2.2462	0.8252
25.06	2.2309	0.8196
27.57	2.2097	0.8118
25.06	2.2241	0.8171
23.81	2.2293	0.8190
22.56	2.2401	0.8232
21.30	2.2600	0.8303
20.05	2.2783	0.8370
18.80	2.2876	0.8404
17.54	2.2936	0.8426
15.04	2.3059	0.8471
12.53	2.3197	0.8522
10.03	2.3352	0.8579
7.52	2.3502	0.8634
7.02	2.3630	0.8681
6.77	2.3617	0.8676
6.52	2.3789	0.8740
5.01	2.4162	0.8877
4.56	2.4751	0.9093
2.51	2.5229	0.9268
1.11	2.5665	0.9429
0.90	2.7030	0.9930
0.00	2.7220	1.0000

Table AXV. Isothermal compressibility of West Lebanon glacial till specimen 40.

n = 0.354 S_i = 57.3%

Pressure kbars	Volume cm^3	Relative Volume
0.00	2.7390	1.0000
0.12	2.5510	0.9314
0.38	2.4704	0.9019
0.63	2.4214	0.8841
1.25	2.3503	0.8583
1.63	2.3123	0.8444
1.88	2.2874	0.8351
2.51	2.2596	0.8250
3.76	2.2328	0.8152
6.00	2.2049	0.8050
6.09	2.1930	0.8007
7.52	2.1720	0.7930
8.27	2.1707	0.7925
8.77	2.1493	0.7847
10.03	2.1406	0.7815
12.53	2.1324	0.7785
15.04	2.1251	0.7759
17.54	2.1165	0.7727
20.05	2.1104	0.7705
22.56	2.1035	0.7680
25.06	2.0967	0.7655
26.32	2.0930	0.7642
26.94	2.0880	0.7623
25.07	2.0730	0.7569
22.56	2.0846	0.7611
20.05	2.0933	0.7642
17.54	2.1006	0.7669
15.04	2.1054	0.7687
12.53	2.1148	0.7721
10.03	2.1222	0.7748
6.92	2.1328	0.7787
6.52	2.1546	0.7866
5.01	2.1707	0.7925
4.39	2.2006	0.8034
2.51	2.2308	0.8145
1.33	2.2555	0.8235
0.38	2.3267	0.8495
0.00	2.3415	0.8549

Table AXVI. Isothermal compressibility of West Lebanon glacial till specimen 16.

n = 0.357 S_i = 58.3%

Pressure kbars	Volume cm^3	Relative Volume
0.00	2.7330	1.0000
0.50	2.4356	0.8912
1.00	2.3037	0.8429
1.50	2.2643	0.8285
2.51	2.2340	0.8174
5.01	2.2062	0.8072
6.27	2.1902	0.8014
6.77	2.1729	0.7947
7.52	2.1560	0.7889
9.02	2.1422	0.7838
11.[illegible]	2.1289	0.7790
20.05	2.1036	0.7697
22.56	2.0959	0.7669
25.06	2.0919	0.7654
27.57	2.0781	0.7606
25.06	2.0793	0.7610
22.56	2.0844	0.7627
20.05	2.0954	0.7667
12.53	2.1101	0.7721
6.77	2.1408	0.7833
5.51	2.1683	0.7934
4.51	2.1837	0.7990
4.26	2.1974	0.8040
1.00	2.2532	0.8244
0.50	2.3043	0.8431
0.00	2.3165	0.8476

Table AXVII. Isothermal compressibility of West Lebanon glacial till specimen 32.

n = 0.354 S_l = 100%

Pressure kbars	Volume cm^3	Relative Volume
0.00	2.7540	1.0000
0.65	2.7398	0.9948
1.25	2.6166	0.9501
1.50	2.6009	0.9444
2.51	2.5710	0.9335
3.76	2.5438	0.9237
4.94	2.5247	0.9167
5.26	2.4795	0.9003
5.76	2.4666	0.8956
6.57	2.4571	0.8922
7.02	2.4304	0.8825
7.52	2.4263	0.8810
10.03	2.4115	0.8756
12.53	2.3985	0.8709
15.04	2.3866	0.8666
17.54	2.3750	0.8624
20.05	2.3657	0.8590
22.56	2.3552	0.8552
23.31	2.3455	0.8517
24.31	2.3321	0.8468
25.06	2.3157	0.8403
26.32	2.3057	0.8372
28.32	2.2984	0.8346
22.56	2.3257	0.8445
21.30	2.3268	0.8449
20.05	2.3557	0.8554
19.30	2.3677	0.8597
17.54	2.3750	0.8624
15.04	2.3866	0.8666
12.53	2.3985	0.8709
10.03	2.4115	0.8756
7.52	2.4263	0.8810
7.02	2.4304	0.8825
6.27	2.4369	0.8848
6.02	2.4561	0.8918
5.76	2.4666	0.8956
4.76	2.4827	0.9015
4.51	2.5060	0.9099
4.26	2.5231	0.9161
3.76	2.5430	0.9234
2.51	2.5710	0.9335
1.50	2.6009	0.9444
1.25	2.6166	0.9501
0.65	2.7391	0.9948
0.00	2.7540	1.0000

Table AXVIII. Isothermal compressibility of West Lebanon glacial till specimen 42.

n = 0.358 S_l = 100%

Pressure kbars	Volume cm^3	Relative Volume
0.00	2.7230	1.0000
0.83	2.7032	0.9927
1.33	2.5825	0.9484
1.75	2.5599	0.9401
2.51	2.5363	0.9316
4.01	2.5013	0.9186
4.89	2.4807	0.9110
5.01	2.4357	0.8945
6.42	2.4154	0.8870
6.77	2.3826	0.8750
7.52	2.3754	0.8724
10.03	2.3593	0.8664
12.53	2.3448	0.8611
15.04	2.3314	0.8562
17.54	2.3191	0.8517
20.05	2.3094	0.8481
21.30	2.3039	0.8461
22.56	2.2906	0.8412
23.31	2.2601	0.8300
25.06	2.2471	0.8252
27.70	2.2343	0.8205
25.06	2.2437	0.8240
22.56	2.2503	0.8264
21.30	2.2671	0.8326
20.05	2.3000	0.8446
18.30	2.3149	0.8501
17.54	2.3191	0.8517
15.04	2.3314	0.8562
12.53	2.3448	0.8611
10.03	2.3593	0.8664
7.52	2.3754	0.8724
6.77	2.3826	0.8750
6.42	2.4154	0.8870
5.01	2.4357	0.8945
4.63	2.4751	0.9084
4.01	2.5013	0.9186
2.51	2.5363	0.9316
1.75	2.5599	0.9401
1.33	2.5825	0.9484
0.83	2.7032	0.9927
0.00	2.7230	1.0000

DOCUMENT CONTROL DATA - R & D

(Security classification of title, body of abstract and indexing annotation must be entered when the overall report is classified)

1. ORIGINATING ACTIVITY (Corporate author) U.S. Army Cold Regions Research and Engineering Laboratory Hanover, N.H. 03755	2a. REPORT SECURITY CLASSIFICATION Unclassified
	2b. GROUP

3. REPORT TITLE

THE ISOTHERMAL COMPRESSIBILITY OF FROZEN SOIL AND ICE TO 30 KILOBARS AT -10°C

4. DESCRIPTIVE NOTES (Type of report and inclusive dates)

5. AUTHOR(S) (First name, middle initial, last name)

Edwin Chamberlain and Pieter Hoekstra

6. REPORT DATE	7a. TOTAL NO. OF PAGES	7b. NO. OF REFS
June 1970	38	19

8a. CONTRACT OR GRANT NO.	9a. ORIGINATOR'S REPORT NUMBER(S) Technical Report 225
b. PROJECT NO. ARPA Order 968	
c.	9b. OTHER REPORT NO(S) (Any other numbers that may be assigned this report)
d.	

10. DISTRIBUTION STATEMENT

This document has been approved for public release and sale; its distribution is unlimited

11. SUPPLEMENTARY NOTES	12. SPONSORING MILITARY ACTIVITY
	Advanced Research Projects Agency Washington, D.C. 20301

13. ABSTRACT

The isothermal compressibilities of ice and partially and fully saturated sand and silt at -10°C are presented. The tests employ a piston-die device with which a uniaxial load is imposed on a lead encapsulated specimen, resulting in the hydrostatic compression of the test specimen. Pressures to 30 kbars are obtained. The compressibility of ice is as reported by P.W. Bridgman. The various phase transformations of ice I to water to ice V to ice VI to ice VIII appear as expected. It is shown that the compressibility of frozen soil can be readily predicted from the knowledge of material properties such as degree of saturation with ice, porosity, and the compressibilities of the ice and mineral components.

14. KEYWORDS

Isothermal compressibility of frozen soils
Isothermal compressibility of ice